UNIVERSIDADE DE LISBOA

FACULDADE DE CIÊNCIAS

DEPARTAMENTO DE FÍSICA

Reproducibility and sensitivity of brain network backbones: a demonstration in Small Vessel Disease

Beatriz Esteves Padrela

Mestrado Integrado em Engenharia Biomédica e Biofísica

Perfil em Sinais e Imagens Médicas

Dissertação orientada por:

Professor Eduardo Ducla-Soares, Faculdade de Ciências da Universidade de Lisboa

Professor Doctor Geert Jan Biessels, University Medical Center Utrecht

2020

'Learning is the only thing the mind never exhausts, never fears, and never regrets.'

-Leonardo Da Vinci

Acknowledgements

First of all, I want to express my deepest gratitude to all those who provided me the opportunity to carry out this internship and work in an exceptional research team. I want to thank Erasmus+ for giving me this opportunity and to VCI director, Pr. Dr. Geert Jan Biessels, for always making me feel secure of my capabilities and for providing an extremely good spirit of fellowship between the group.

To my supervisor Bruno Robalo, I really want to thank you for all the patience, continuous guidance and your smart and clear way of explaining science, which could only have come from an equally intelligent person and talented professional, providing me an incredible experience of learning Physics. Thank you for everything, I was very lucky. I also want to thank my internal supervisor, Pr. Eduardo Ducla-Soares, for all the valuable inputs for my work and for always being so helpful.

I am also grateful to the entire VCI group for the incredible work environment and for all the joyful times that made work easier, especially my office mate, Angelina Kancheva, thank you for your friendship and support. I would also like to thank the Erasmus+ scholarship without which my stay in Utrecht wouldn't have been possible.

I would also like to thank my friends and family for all the support, love and friendship. Em primeiro lugar, agradecer aos meus amigos que passaram comigo estes seis meses incríveis na Biltstraat: João, Sousa, Neto, Bia e Inês, com quem vivi momentos tão bons e inesquecíveis. Desde as máquinas de lavar, às noites no jardim, aos filmes, jantaradas e bolachas (digestivas também). Quero também agradecer à house lady Else, for always reminding me to clean the sink and for always giving a warmful "have a nice meal" appearing from nowhere. À minha melhor amiga Mónica, pela amizade incondicional, por me aturar sempre e estar sempre lá para mim durante estes 5 loucos anos; e obv, por me fazer rir até doer a barriga e cantar comigo até de madrugada. À minha querida amiga Pipa, pelos momentos que passámos nestes anos todos e por estarmos juntas desde o dia 1, nas aulas e fora delas. E claro, ao meu querido João, por todo o amor e amizade, pelo apoio que me deu nos momentos mais difíceis e por me fazer tão feliz todos os dias.

Finalmente, à minha família, um agradecimento especial. Aos meus irmãos João, Rita e Marta, pelo vosso amor e por acreditarem em mim todos os dias. Não teria conseguido fazer nada sem vocês ao meu lado! Sou muito sortuda por vos ter. Aos meus queridos avós: avó Mimi, avó Emília e avô Herculano por todo o apoio, carinho e amor incondicional que sempre tiveram para me dar. Ao meu tio Miguel, que tantas saudades tenho, por ter sido uma das razões de me querer tornar uma cientista. Ao meu primo Pedro, por ter sido sempre um dos meus grandes suportes e por nunca ter deixado de acreditar em mim e naquilo que sou capaz. E finalmente aos meus pais, Paulo e Susana, por serem o meu porto de abrigo e pela educação e amor incondicional que me deram desde pequena, que também me fizeram chegar até aqui. Por acreditarem sempre nas minhas capacidades desde o primeiro dia, e por estarem lá sempre para mim aconteça o que acontecer.

Abstract

Whole-brain networks have been used to study the connectivity paths within the brain, constructed using information from diffusion magnetic resonance imaging (dMRI) data and white matter fiber tractography (FT). These techniques can detect alterations in the white matter integrity and changes in axonal connections, whose alterations can be due to the presence of small vessel disease (SVD).

However, there is a lack of consensus in network reconstruction methods and therefore no gold-standard model of the human brain network. Moreover, dMRI data are affected by methodological issues such as scan noise, presence of false-positive and false-negative connections. Consequently, the reproducibility and the reliability of these networks is normally very low.

A potential solution to deal with the low reproducibility of brain networks is to analyze only its backbone structure. This backbone is assumed to represent the building blocks of structural brain networks and thus composed by a set of strong connections and voided of spurious connections. Such backbone should be reproducible in scan-rescan scenarios and relatively consistent between healthy subjects, while still being sensitive to disease-related changes. Several types of backbones have been proposed, constructed using white matter tractography, with dMRI data. However, no study has directly compared these backbones in terms of reproducibility, consistency, or sensitivity to disease effects in a patient population.

In this project, we examined: (1) whether the proposed backbones can be applied to clinical datasets by testing if they are reproducible over two time-points and consistent between groups; (2) if they are sensitive to disease effects both in a cross-sectional and longitudinal analysis. We evaluated our research questions on a longitudinal cohort of patients with cerebral SVD and age matched controls, as well as a validation dataset of healthy young adults. Our cohort contained 87 elderly memory clinic patients with SVD recruited via the UMC Utrecht, scanned twice with an inter-scan time between baseline and follow-up of 27 ± 4 months. We also included baseline scans of 45 healthy elderly, matched in age, sex and education level, to be used as controls. Data from 44 healthy young adults was used as validation data. For each subject, we reconstructed brain structural networks from the diffusion MRI data. Subsequently, we computed 4 types of network backbone, previously described in literature: the Minimal Spanning Tree (MST), the Disparity Core, the K-Core, and Hub-Core.

We compared these backbones and tested their reproducibility within subjects, and their consistency across subjects and across groups. Moreover, we performed a cross-sectional analysis between controls and patients at baseline, to evaluate if these backbones can detect disease effects and a longitudinal analysis with patient data over time, to test if they can detect disease progression. Regarding our first objective, our results show that overall MST is the backbone that shows the best reproducibility between repeated scans, as well as the highest consistency among subjects, for all of the three brain templates that we used. Secondly, the MST was also sensitive to network alterations both on a cross-sectional analysis (patients vs. controls) and on a longitudinal analysis (baseline vs. follow-up).

We therefore conclude that, the use of these network backbones, as an alternative of the whole-brain network analysis, can successfully be applied to clinical datasets as a novel and reliable way to detect disease effects and evaluate disease progression.

Key-words: small vessel disease, diffusion tensor imaging, fiber tractography, white matter, neural network, brain connectivity, network backbone.

Resumo

A demência vascular cerebral (SVD) é a segunda principal causa de demência, depois da doença de Alzheimer. Este tipo de demência está relacionado com patologias vasculares cerebrais, assim como com perda de funcionalidades cognitivas. Vários estudos explicam que a degradação da atividade cognitiva característica desta doença pode dever-se à diminuição da integridade da substância branca e a alterações nas conexões axonais. O estudo da conectividade cerebral tem sido uma forte aposta no estudo das causas e da forma como a demência vascular cerebral evolui.

A construção de mapas neuronais é uma das práticas que mais tem sido usada para estudar e entender os mecanismos principais da conectividade cerebral: representar o cérebro como um conjunto de regiões e as ligações entre elas. Para isso, utiliza-se informação proveniente de imagens de ressonância magnética por difusão (dMRI), especificamente de imagens por tensor de difusão (DTI), capazes de medir a magnitude de difusão das moléculas de água no cérebro *in vivo*, através de gradientes aplicados em pelo menos seis direções no espaço. Desta forma, é possível estimar a direção principal do movimento das moléculas de água que compõem as microfibras da substância branca cerebral, e reconstruir os percursos de neurónios que conectam as várias regiões do cérebro. Este processo é chamado de tractografia de fibras (FT), que proporciona um modelo a três dimensões da arquitetura tecidular cerebral, permitindo a visualização e o estudo da conectividade e da continuidade dos percursos neuronais. Assim, é possível obter informação quantitativa acerca do sistema nervoso *in vivo* e contruir mapas de conectividade cerebral.

No entanto, existe falta de consenso sobre as regras de reconstrução destes mapas neuronais, fazendo com que não haja um modelo-base para o estudo dos mesmos. Além disto, os dados provenientes das imagens de dMRI são facilmente afetados e podem diferir da realidade. Alguns exemplos mais comuns são a presença de ruído e existência tanto de conexões falsas como a ausência de conexões que deviam estar presentes, chamadas respetivamente de falsos-positivos e falsos-negativos. Consequentemente, os modelos de conectividade não podem ser comparados entre diferentes aparelhos de ressonância, nem mesmo entre diferentes momentos temporais, por terem uma baixa reprodutibilidade, tornando estes métodos poucos fiáveis.

As soluções propostas para lidar com esta falta de consenso quanto à reconstrução de mapas ou redes neuronais e a presença de conexões falsas podem ser agrupadas em duas categorias: normalização e redução da rede neuronal através da aplicação de um limiar (threshold, em inglês). Contudo, os processos de normalização para remover certas tendências erradas destas redes não eram suficientes e, por vezes, introduziam outras dependências. Quanto à aplicação de limiares, mesmo que alguns estudos mostrem que a sua utilização no mapa neuronal do cérebro todo pode efetivamente eliminar alguns efeitos, a própria escolha de um limiar pode conduzir a modificações nas redes neuronais através de eliminação de certas comunicações fundamentais.

Como uma extensão da redução destas redes neuronais com o objetivo de lidar com a sua baixa reprodutibilidade, vários estudos têm proposto uma nova abordagem: analisar apenas uma espécie de esqueleto das mesmas. O objetivo deste "esqueleto-neuronal" é o de representar as ligações mais importantes e estruturais e estar isento de falsas conexões. Idealmente, este "esqueleto-neuronal" seria reprodutível entre diferentes dispositivos e consistente entre indivíduos saudáveis, enquanto se manteria fiel às diferenças causadas pela presença de doenças. Assim sendo, o estudo da extração de um esqueleto-neuronal, visa encontrar estruturas fundamentais que evitem a perda de propriedades topológicas. Por

exemplo, considerando pacientes com SVD, estes esqueletos-neuronais devem fornecer uma melhor compreensão das alterações da conectividade cerebral ao longo do tempo, permitindo uma comparação sólida entre diferentes pontos no tempo e a identificação de alterações que sejam consequência inegável de doença. Alguns tipos destas redes neuronais foram já propostos em diversas publicações científicas, que podem ser construídos utilizando FT de substância branca com informação proveniente de dMRI. Neste estudo, utilizamos o Minimum Spanning Tree (MST), o K-Core, o Disparity Core e o Hub-Core, que são redes-esqueleto já existentes na literatura. A eficácia tanto do uso do MST como do K-Core já foram comprovadas tanto a nível de deteção de alterações da conectividade cerebral, como na medida em que conseguem manter as conexões mais importantes do esqueleto cerebral, eliminando conexões que podem ser consideradas duvidosas. No entanto, até agora, nenhum estudo se focou na comparação dos diferentes esqueletos-neuronais existentes quanto à sua reprodutibilidade, consistência ou sensibilidade aos efeitos de doença ao longo do tempo.

Neste estudo, utilizamos os quatro modelos-esqueletos mencionados anteriormente, avaliando: (1) se estes esqueletos-neuronais podem ser efetivamente aplicados a dados clínicos, testando a sua reprodutibilidade entre dois pontos de tempos distintos e a sua consistência entre grupos de controlos saudáveis; (2) se são sensíveis a efeitos causados por doença, tanto entre controlos e pacientes, como na evolução de alterações de conectividade em pacientes ao longo do tempo. Os dados longitudinais utilizados provêm de imagens ponderadas em T1 de 87 pacientes idosos com SVD, assim como de um grupo controlo de 45 idosos saudáveis coincidentes em idade com estes pacientes, e de um grupo de validação constituído por 44 jovens saudáveis. Para cada um dos objetivos, testamos os 4 tipos de esqueletos-neuronais, baseados primeiramente num modelo que divide o córtex cerebral em 90 regiões de interesse (ROIs) e posteriormente em modelos de 200 e 250 regiões. No pós-processamento, foram construídas e comparadas matrizes de conectividade que representam as ligações entre as várias regiões em que dividimos o córtex. Com estas matrizes foi possível calcular valores de conectividade como a força nodal (NS) e a eficiência global (GE). Também foram comparadas matrizes que diziam respeito a parâmetros específicos de DTI como a anisotropia fracionada (FA) e a difusividade média (MD). A análise estatística foi feita utilizando testes paramétricos t-test e ANOVA.

Os resultados indicam que, no geral, estas redes podem ser utilizadas como forma de analisar e estudar mapas de conectividade cerebral de forma mais precisa, pois são reprodutíveis entre controlos saudáveis em tempos diferentes, e conseguem detetar as diferenças de conectividade devidas a doença. Além disso, representam as ligações mais importantes da rede de conectividade neuronal, criando uma base para comparações fiáveis. A maior parte dos esqueletos-neuronais mostraram ser consistentes dentro de cada grupo de estudo, e apresentaram diferenças de conectividade entre controlos e pacientes. Neste caso, comparando sujeitos saudáveis com pacientes, os valores das componentes de FA e de MD destes esqueletos neuronais, e as suas alterações, vão de encontro com a literatura sobre a evolução do estado das ligações neuronais no desenvolvimento de demência. Quanto à análise longitudinal dos pacientes, concluímos que a NS representa uma medida mais fiável de análise das alterações ao longo do tempo da doença do que a GE. Finalmente, e ainda que algumas destes esqueletos-neuronais tenham mostrado melhor desempenho do que outros em diferentes abordagens, concluímos que o MST é a rede-esqueleto que dispõe dos melhores resultados utilizando o modelo de 90 e 200 ROIs, do cérebro todo, assim como usando o modelo de 250 ROIs aplicado só ao hemisfério esquerdo.

Em suma, conclui-se que a utilização destes tipos de redes-esqueleto pode vir a tornar-se uma melhor alternativa em relação à utilização das redes neuronais originais do cérebro completo, visto que

podem ser eficazmente aplicadas à análise de dados clínicos como forma fiável de detetar presença e evolução de doenças.

Palavras-chave: demência vascular, tractografia, substância branca, conectividade cerebral, esqueleto-neuronal.

Contents

List of Figures

List of Tables

List of Abbreviations

AAL – Automated Anatomical Labelling

ADC - Apparent Diffusion Coefficient

BC - Betweenness Centrality

CDR - Clinical Dementia Rating

CNS - Central Nervous System

CSD - Constrained Spherical Deconvolution

CT - Computerized Tomography

DT – Diffusion Tensor

DTI – Diffusion Tensor Imaging

DWI – Diffusion Weighted Imaging

FA – Fractional Anisotropy

FLAIR – Fluid-Attenuated Inversion Recovery

fODF - Fiber Orientation Distribution Function

FT – Fiber tractography

GE – Global Efficiency

GM – Grey matter

HS – Hub Score

HCP – Human Connectome Project

ICV – Intracranial Volume

MMSE – Mini Mental State Examination

MRI – Magnetic Resonance Imaging

MST – Minimum Spanning Tree

NOS – Number of Streamlines

NS – Node Strength

PGSE - Pulsed Gradient Spin Echo

RF - Radiofrequency

ROI – Region of Interest

SD – Standard Deviation

SVD – Small Vessel Disease

TE – Echo Time

TI – Inversion Time

WMH – White Matter Hyperintensities

1. Introduction

Diffusion Magnetic Resonance Imaging (dMRI) is an advanced neuroimaging technique and can detect brain lesions by identifying alterations in white matter integrity and changes in axonal properties[1]. These alterations are associated with cognitive dysfunction and dementia[2], leading to neurodegenerative processes such as cerebral small vessel disease (SVD), which is a vascular brain pathology[3–5]. Diffusion tensor imaging (DTI), as an extension of diffusion-weighted imaging (DWI), is a magnetic resonance (MR) technique capable of measuring the magnitude of diffusion of water molecules within tissues. By using diffusion information, it is possible to use tractography to map intra- and inter-cortical pathways and model the human brain as networks or graphs *in vivo*[6]. Thus, DTI can be used to study connectivity changes, specifically white matter microstructure changes due to small vessel disease[2,7–9].

However, despite these advances in neuroscience, there are still methodological issues that remain unsolved[10,11]. Brain networks are widely used to describe the brain as a set of regions, called nodes, and the connections between them, called edges. Moreover, representing the brain as a network as already been proved to be efficient in detecting cognitive changes due to cognitive impairment, by studying the network measures[12–15]. Nevertheless, there is a lack of consensus in network reconstruction methods and therefore no gold-standard model of the human brain network. Researchers use different tractography algorithms and different brain parcellations[16,17], which makes it difficult to harmonize results from different studies[10,18]. Moreover, dMRI provides indirect measurements, and the accuracy of white matter tractography is very dependent on methodological factors[19], such as noise and other artefacts, leading to the presence of false-positive and false-negative connections. The above mentioned issues have limited comparability among experimental conditions, cohorts and studies[20].

The solutions proposed to deal with the lack of consensus in network reconstruction and the presence of spurious connections can be grouped into two categories: 1) normalization and 2) network reduction by applying a threshold. Normalization typically involves comparison of estimated network characteristics to a reference network with the same density (percentual number of connections), and sometimes also the same degree distribution (number of connections of the network nodes) [20]; whilst network reduction involves removing potential false positive connections from the network by means of thresholding. However, normalization can sometimes introduce other dependencies[18], and although some studies show that thresholding applied to the whole brain network can actually eliminate size and density effects[21–23], choosing threshold conditions may lead to modifications of the network by enforcing or ignoring connections[18].

In order to solve this problem, studies have proposed a new approach: to only analyze the backbone structure of the network[10,24]. Network backbones are types of brain networks that do not use the entire information of the whole-brain connectivity network. The backbone should represent the building blocks of structural brain networks and could be used as a null model of connections, in order to provide a reference model for brain analysis and detect disease-related changes. Considering patients with SVD, these backbones should provide a better understanding of altered connectivity over time, allowing a robustly comparison between time-points and identifying alterations due to disease.

Several types of backbones have been proposed in literature. Analysis of the **Minimum Spanning Tree (MST)** has shown to be a viable method to directly compare structural brain networks of different populations[20]. The MST is defined as the sub-network that connects all nodes within the network, as efficiently as possible, without forming any loops[20]. Previous studies have shown that MST analysis can be used to capture network alterations due to aging and disease in both functional and structural imaging data[13,20,25,26]. The **K-Core decomposition** consists in identifying particular subsets of the graph, called k-cores, obtained by removing all the nodes of degree smaller than k, until the degree of all remaining nodes is larger than or equal to k. Nodes with larger degree and more central position in the structure of the network correspond to larger values of the index k[27]. The K-Core was found to be a useful extraction of the overall brain network[14] compared to the full connectivity matrix, eliminating the least reliable connections which can arise due to tract tracing errors. Its anatomical correspondence with regions of high metabolic activity and with some elements of the human default network suggests that this backbone may be an important structural basis for shaping large-scale brain dynamics[28].

The third backbone is called **Disparity Core**, that is a local filter. It goes to each node individually, and it proceeds by identifying which connections for each node should be preserved in the network, based on the local identification of the statistically relevant weight heterogeneities, and is able to filter out the backbone of dominant connections in weighted networks with strong disorder, maintaining structural properties and hierarchies at all scales[24]. Finally, the **Hub Core** is a network backbone based on high-centrality nodes[16], called hubs. This sub-network uses the strongest network hubs, maintaining all their connections. Detailed information about these backbones, can be found in Section 2.5.3. Excluding the Disparity Core, all the others have already been applied to the study of the brain.

Our goal focuses on evaluating which of these network backbones are a better representation of the brain structure and if they can be applied to clinical datasets. This thesis focuses on the following questions: 1) Are these backbones reproducible over time? 2) Are they sensitive to disease effects in cross-sectional analysis and to disease progression in longitudinal analysis? Moreover, we compare weighted graph measures of global and local connectivity, by using a test-retest dataset of 87 elderly memory clinic patients with SVD, from Parelsnoer study[29]; 44 young healthy subjects, used as validation data, provided by the Human Connectome Project[30], also from two distinct time-points; and we also included baseline scans of 45 healthy elderly, matched in age, sex and education level, provided by the Utrecht Diabetic Encephalopathy Study (UDES)[31], to be used as controls. In order to define the brain regions used for the analysis, we primarly used a subset of the 90 non-cerebellarregions-of-interest composing the automated anatomical labelling (AAL) parcellation atlas[17] for all of our subject groups on both time-points. Afterward, we performed the analysis with a 200-nodes whole-brain parcellation and a 250-nodes left hemisphere parcellation based on a study by Schaefer *et al*[32]., used only for the validation data at baseline.

This manuscript is divided in 6 chapters. The theoretical background necessary to understand this work is introduced in chapter 2, including concepts such as SVD, DWI and DTI, fiber tractography, brain connectomics, network reconstruction and graph theory. Then, in the methods (chapter 3), it is explained how the network backbones were reconstructed for each template, of 90, 200 and 250 nodes, as well as all the techniques used. The results of this study are presented in chapter 4 and discussed in chapter 5. General conclusions are provided in chapter 6.

2. Background

2.1. Vascular Cognitive Impairment

Vascular cognitive impairment (VCI) refers to the spectrum of vascular brain pathologies that contribute to any degree of cognitive impairment, ranging from subjective cognitive decline to dementia[5]. VCI can be caused by stroke affecting large blood vessels, but is mainly caused by small vessel disease[3,33,34]. For that reason, deterioration can be slow and gradual, that is, stepwise deterioration and focal cognitive deficits are often not observed[5].

2.1.1. Small Vessel Disease

Cerebral small vessel disease affects the small blood vessels deep within the brain, causing damage to deep (subcortical) areas. SVD is responsible for 10%–30% of stroke cases and 50%–70% of vascular cognitive impairment[35]. This damage to the blood vessel walls can be a consequence of untreated high blood pressure or diabetes leading to vascular disease.

The main cerebrovascular pathologies in VCI are infarcts and white matter hyperintensities (WMHs)[5], that are types of small vessel lesions seen on neuroimaging where the brain is most damaged. The resulting brain damage can also include lacunes (small strokes resulting in fluid-filled spaces)[3] and cerebral microbleeds (flow voids in pial blood vessels in cortical sulci)[36]. These lesions (Figure 2.1) might be clinically silent individually, as many affected people do not have symptoms. However, increasing numbers of both individual lesions and combinations of SVD lesion types are associated with cognitive impairment, dementia, depression, mobility problems, increased risk of stroke[37] and worse outcome after stroke[38]. Fortunately, brain scanning techniques such as magnetic resonance imaging (MRI) or computerized tomography (CT) can detect the presence of these vascular injuries.

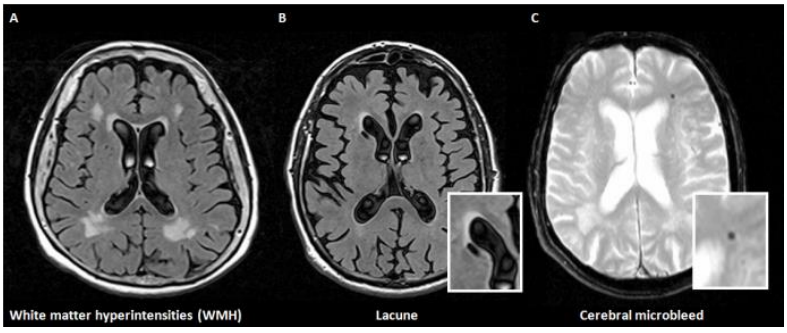

Figure 2.1 *- Conventional MRI Brain lesions can include white matter hyperintensities (A), lacunes (B) and microbleeds (C). Image from a paper of van der Holst*[39].

In terms of diagnosis of VCI, the key requirements are (1) demonstration of a cognitive deficit by neuropsychological testing and (2) presence of cerebrovascular disease. In the first place, a cognitive test has to be performed, involving a minimum of 4 cognitive domains: executive/attention, memory,

language, and visuospatial functions[33]. Equally important is the presence of cerebrovascular pathologies, which can be determined by the extent, location and type of vascular lesions, with MRI and CT techniques. MRI should include T1-weighted imaging to detect atrophy, T2-weighted imaging to detect lacunar infarcts and fluid-attenuated inversion recovery (FLAIR) sequences to detect WMHs[5]. In addition, diffusion tensor imaging (DTI) can detect changes in the white matter (WM) tracts[5].

Some types of nerves damage include demyelination, in which the myelin sheath of neurons is damaged, impairing the conduction of signals in the affected nerves; and gliosis, that involves the proliferation or hypertrophy of glial cells in response to damage to the central nervous system (CNS). Histopathological examination of WMHs in a study by Gouw *et al.*[40], showed different degrees of demyelination, gliosis and loss of nerve fibers. Therefore, as the white matter tracts are crucial for information transfer between brain regions, it may result in a lower structural network efficiency, and consequently, worse cognitive performance. A presumed mechanism is that SVD disturbs the structural connectivity within a large-scale brain network, thereby impairing the ability of the brain to integrate the neural processes efficiently[41]. Several MRI studies have looked at the relationship between vascular lesions, structural connectivity, and cognitive function, with most work done in patients with cerebral SVD. These studies consistently found an association between the burden of SVD-related brain lesions and reduced global network efficiency[41–43], a parameter that will be explored in the Section 2.5.1. Therefore, studying the brain connectivity can be crucial to understand the mechanisms through which SVD lesions affect cognition, and eventually lead to cognitive impairment.

Furthermore, the aforementioned conventional MRI techniques, coarsely dichotomize tissue between normal and abnormal, and do not reliably reflect the degree of demyelination[44], while quantitative imaging techniques, including DTI, can provide a detailed evaluation of the underlying tissue alterations at the voxel level[34,39].

Thus, recently, dMRI, fiber tractography and brain network analysis have been applied to explore and understand the underlying mechanisms of VCI.

2.2. DIFFUSION TENSOR IMAGING (DTI)

Diffusion tensor imaging is an MRI technique that is sensitive to microstructural tissue changes as it measures the magnitude and direction of diffusion of water molecules. Therefore, it is popular for imaging the white matter fiber tracts of the brain, and it has been applied to a variety of neuroscientific studies including autism[45], schizophrenia[46], dementia[47] and aging[48].

2.2.1. Principles of Diffusion

Water molecules, in our body, undergo random translational motion. In physics, this motion is called Brownian Motion, as Robert Brown[49] discovered in 1827 that all molecules in a fluid warmer than absolute zero have thermal energies that cause them to show random motion. This movement, also called diffusion, was later described by Einstein[50] with the well-known diffusion equation:

$$\langle x^2 \rangle = 2Dt_d \tag{2.1}$$

explaining the relation between the mean-squared displacement $\langle x^2 \rangle$ (m^2) of the particle during a diffusion time t_d (s) and the diffusion coefficient D $(m^2 \cdot s^{-1})$.

However, in this example, the mean-squared displacement $\langle x^2 \rangle$ is independent of the direction in which particles move (isotropic diffusion), that is, the diffusion would be the same in all directions. In an inhomogeneous medium (ie, structured in some way), the particles do not diffuse equally in all directions, so the diffusion measured in tissue varies with direction (anisotropic diffusion). In white matter, diffusion anisotropy is primarily caused by cellular membranes, with some contribution from myelination and the packing of axons[51,52]. Therefore, anisotropic diffusion can indicate the underlying tissue orientation.

Diffusion MRI can make this distinction, by replacing D in the equation by the apparent diffusion coefficient (ADC) for each measured direction.

2.2.2. Measurement of diffusion with MRI

Diffusion-weighted imaging (DWI) was then introduced in the mid-1980s[53], as a magnetic resonance imaging technique for evaluating tissue pathophysiology in vivo based on the measure of the random motion of water molecules[54]. In order to understand the principles of dMRI, we first need a brief introduction to MRI and the way the measurement is done.
Hydrogen, present in water molecules, is naturally abundant in humans, and its protons can be excited by magnetic fields. To produce a typical image, an MRI scanner starts with the alignment of the spin of protons in water molecules to the magnetic field B_0 of the equipment, making them rotate with a frequency directly proportional to the field strength.

Then, the excitation of the nuclei radiofrequency (RF) pulse, rotates the magnetization vector into the plane normal to the main magnetic field (90º pulse), or into an antiparallel position (180º pulse), creating a state of disequilibrium. When the RF pulse is turned off, the orientation of the spins realigns with the magnetic field B_0 via an exponential decay. This process is called Relaxation. During this process, as protons are returning to equilibrium, they release energy that can be detected by the scan sensors. The

amount of energy released, and the recovery time, will be characteristic of the tissue it is part of. Furthermore, by varying the excitation and dephasing of the nuclei, it is possible to measure tissue properties like the local change in oxygenation (functional MRI) and the diffusion of water molecules (diffusion MRI).

Stejskal and Tanner introduced in 1964 a description of a DW-MR sequence, called Pulsed gradient spin echo (PGSE). This MRI sequence is based on the normal spin echo (SE) sequence, including a 180º RF pulse following a 90º pulse, with an additional pair of high-amplitude diffusion gradients, in order to dephase and, after a spin-echo 180º pulse has been delivered, rephase stationary spins (Figure 2.2).

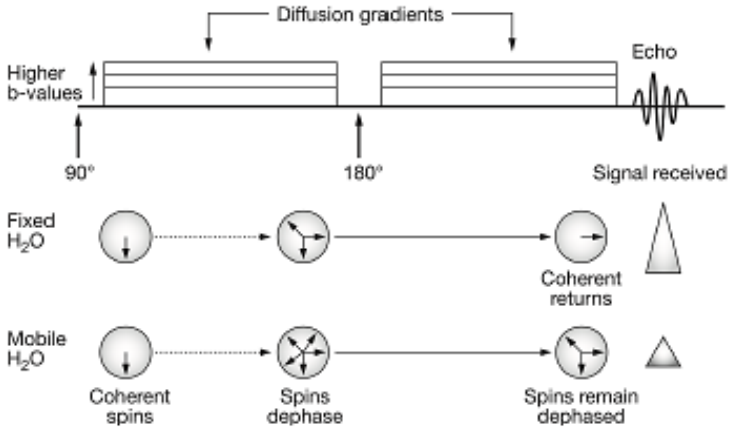

Figure 2.2 - *Representation of Spin Echo Diffusion Weighting Sequence and water spins behavior. As in the classical PGSE sequence, the 90º and 180º RF pulses are applied. In this case, to probe the diffusion behavior of water molecules, two diffusion gradient pulses are applied (top section). In the absence of motion (middle section) the phase offset introduced by the first gradient is cancelled by the second. In the presence of diffusion (bottom section), the second gradient does not cancel the phase offset, producing a signal loss. Image adapted from a paper of Bastiani* et al.[55].

.

After 180º pulse, if there were no changing in the position of the molecule, the only signal loss that will be measured is due to T2 relaxation process. However, if there is motions due to diffusion in the direction of the applied gradients, the individual positions will differ between the application of the first and second diffusion gradients. Therefore, spins that are moving along the direction of the applied diffusion gradient will show bulk dephasing and, consequently, phase loss. This phase loss, due to the diphase of the water molecules in movement, is detected as signal loss, and will be proportional to the amount of diffusion, independent of the T2 relaxation. This phase dispersion characterizes the degree of diffusion weighting, often called *b*-value, is expressed as:

$$b = \gamma^2 \delta^2 |G|^2 \left(\Delta - \frac{\delta}{3}\right) \tag{2.2}$$

where b is the *b*-value measured in s/mm^2, γ is the gyromagnetic ratio, $\delta\ (s)$ is the duration of the diffusion pulse, $|G|\ (T \cdot m^{-1})$ is the amplitude of the diffusion gradient and $\Delta\ (s)$ is the time interval between the two diffusion gradients (Figure 2.3).

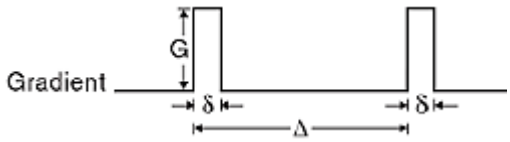

Figure 2.3 *- Schematic representation of the two diffusion gradient pulses. They are characterized by amplitude ($|\boldsymbol{G}|$), duration ($\boldsymbol{\delta}$) and time between their application (Δ). Image adapted from the paper of Johansen-Berg, H. & Behrens,T.*[56]

The decreased signal (S_k) is compared to the original signal (S_0), when no diffusion gradients are applied, to calculate the diffusion tensor (D) by solving the Stejskal-Tanner equation (2.3). In a 3D case, it is the diffusion gradient vector G = (Gx, Gy, Gz) that determines the direction along which diffusion is measured. Moreover, the information contained in the value *b* considers the directions over which the gradient is applied. Therefore, in this case, the *b* is a matrix with the information of the directions of the gradients. This equation describes how the signal intensity at each voxel decreases in the presence of Gaussian diffusion:

$$S_k = S_0 \cdot \exp(-bD) \tag{2.3}$$

In order to create an image that is sensitized to diffusion in a particular direction, a concept of diffusion tensor (DT) was introduced as an extension of DWI, proposed by Peter Basser in 1994[57]. By repeating this process in multiple directions, a three-dimensional diffusion model (the tensor) is estimated:

$$D = \begin{bmatrix} D_{xx} & D_{yx} & D_{zx} \\ D_{xy} & D_{yy} & D_{zy} \\ D_{xz} & D_{yz} & D_{zz} \end{bmatrix} \tag{2.4}$$

This symmetric 3x3 matrix contains six independent components (note that the tensor is symmetric, so $D_{xy} = D_{yx}$, $D_{zx} = D_{xz}$, $D_{yz} = D_{zy}$), as D is measured in at least 6 directions (in addiction to a b0 image), that summarize the diffusion properties of water molecules within a voxel. The diagonal elements are the diffusion variances along axes x,y and z, and, by diagonalizing this diffusion tensor we obtain the eigenvalues ($\lambda_1, \lambda_2, \lambda_3$) and the corresponding eigenvectores (e_1, e_2, e_3)[55].

$$D = \begin{bmatrix} e_{1x} & e_{2x} & e_{3x} \\ e_{1y} & e_{2y} & e_{3y} \\ e_{1z} & e_{2z} & e_{3z} \end{bmatrix}^T \cdot \begin{bmatrix} \lambda_1 & 0 & 0 \\ 0 & \lambda_2 & 0 \\ 0 & 0 & \lambda_3 \end{bmatrix} \cdot \begin{bmatrix} e_{1x} & e_{2x} & e_{3x} \\ e_{1y} & e_{2y} & e_{3y} \\ e_{1z} & e_{2z} & e_{3z} \end{bmatrix} \tag{2.5}$$

The diffusion tensor can be visualized as an ellipsoid (Figure 2.4), showing the probability of the molecules' displacement due to diffusion. The eigenvectors define the directions of the principal axes and the eigenvalues represent the diffusivities in these three directions, respectively. Diffusion is considered isotropic when the eigenvalues are nearly equal (i.e. $\lambda_1 \approx \lambda_2 \approx \lambda_3$).

The major diffusion eigenvector (e_1, direction of greatest diffusivity) is assumed to be parallel to the tract orientation in regions of homogeneous white matter[58], with λ_1 representing its amplitude.

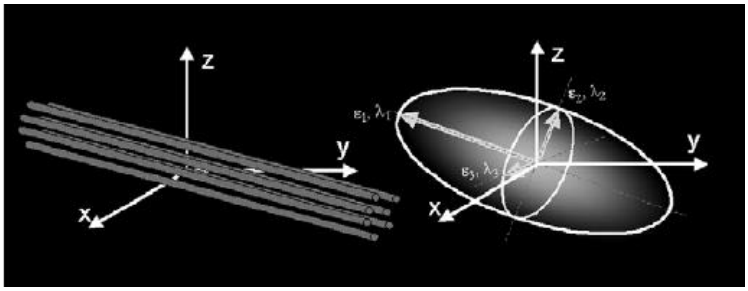

Figure 2.4 - *Schematic representation of the diffusion displacement distributions of the DT. Left: Fiber tracts have an arbitrary orientation with respect to scanner geometry (x,y,z axes) and impose directional dependence (anisotropy) on diffusion measurements. Right: The 3D ellipsoid is based on the values of eigenvectors and eigenvalues, expressing the overall dominant direction of diffusion in that image voxel. Image from Alexander* et al.[58].

This three-dimensional (3D) representation of the diffusion in each voxel, is the basis of diffusion tensor imaging. The information contained in the tensor is represented into 4 numbers (to give an R,G,B color and a brightness value). Consequently, is possible to reconstruct a whole-brain DTI image (Figure 2.5).

2.2.3. DTI measurements

Whilst DTI contains a wealth of information from water diffusion in vivo, analysis often focuses on the extraction of two diffusion metrics: **Mean Diffusivity** (MD), that reflects the average amount of water diffusion in a voxel[59] , equivalent to ADC, is given by:

$$MD = \frac{\lambda_1 + \lambda_2 + \lambda_3}{3} \tag{2.6}$$

Fraction Anisotropy (FA), that determines for each voxel of the image the privileged direction of diffusion, is given by:

$$FA = \sqrt{\frac{3}{2}} \frac{\sqrt{(\lambda_1 - MD)^2 + (\lambda_2 - MD)^2 + (\lambda_3 - MD)^2}}{\sqrt{{\lambda_1}^2 + {\lambda_2}^2 + {\lambda_3}^2}} \tag{2.7}$$

FA represents the fraction of the diffusion tensor that can be assigned to anisotropic (directional) diffusion. Values for FA range between 0 and 1, with higher values reflecting increased directionality of diffusion, independently of the magnitude of diffusion. Lower values are indicating that diffusion is almost the same in all directions (as in Cerebrospinal fluid, CSF) whereas values close to 1 are common along a single direction, such as a fiber tract[1].

In white matter, changes in tissue orientation patterns inside a voxel can result in a change in the degree of anisotropy[60]. Anisotropy measurements may highlight more subtle anomalies in the organization of white matter tracks, e.g., functional disorders that do not necessarily have an anatomical basis[60]. White matter changes such as loss of myelin sheaths and axons are common in Alzheimer's Disease (AD) and may diminish anisotropy[47].

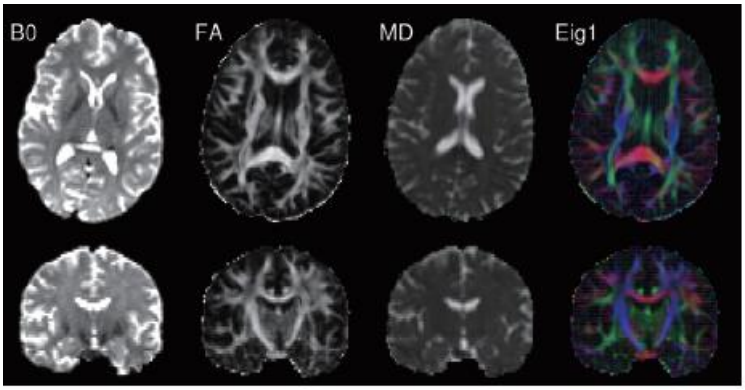

Figure 2.5 - *Diffusion Tensor Imaging. The non-diffusion weighted scan (b0) is shown on the left, followed by the fractional anisotropy (FA) image demonstrating higher values in white matter tracts then the mean diffusivity (MD) image with elevated values in the CSF. The final column shows the direction of principal eigenvector (Eig1) both in color-coded form (red = left/right, green=anterior/posterior, blue=superior/inferior) and in vector form (line segments). Image from Winston* et al., *2012*[61].

As shown in the study of Reijmer *et al.* [2], diffusion MRI can detect changes in WM microstructure and give insight about the type of microstructural damage by looking at changes in MD and FA. Moreover, Bozzali *et al.*[7] showed that white matter hyperintense lesions were detected on scans from patients with Alzheimer's disease. The study explains that diffusion MRI can detect these changes in WM microstructure and give insight about the type of damage by looking at changes in MD and FA. Mayo *et. al.*[62] published a paper which results revealed that individuals with AD, in a longitudinal analysis, had shown reduced FA and increased MD, reflecting loss in myelination and axonal integrity, as a consequence of neurodegeneration[8,9,63]. Furthermore, a study by Selnes *et al.*[64] including 66 dementia patients and 28 normal controls, revealed that FA and MD have been shown to be even better predictors of disease progression in a small patient population, than the levels of tau protein and amyloid beta-42.

Diffusion MRI (dMRI) is then the first noninvasive in vivo imaging modality with the potential to detect these microstructural changes and to generate fiber-tract trajectories in soft fibrous tissues[65], such as white matter of the brain, as explained in the next section.

2.3. FIBER TRACTOGRAPHY

Understanding the anatomy of WM can be very useful to study VCI. By measuring the dMRI signal for each voxel, the local fiber orientations can be pieced together to infer long-range pathways connecting regions of the brain[66], a process known as fiber-tracking or fiber tractography (FT). This provides a three-dimensional reconstruction of the tissue architecture such as the trajectories of white matter fiber bundles[67], by sequentially piecing together the estimates of fiber orientation from the directionality of individual voxels. Thus, FT allows the visualization and study of connectivity and continuity of neural pathways by providing quantitative data of nervous systems in vivo[65]. Two types of tractography have been developed, distinguished by the sampling of fiber directions for streamline propagation. **Deterministic tractography** involves propagating a streamline that follow the principal direction of water diffusion per voxel. This algorithm is based on: (1) user-specified seed point(s), (2) the principal eigenvector of diffusion, as determined by the tensor at each voxel, and (3) user-specified thresholds that restrict the trajectory of the tract[68]. Seed points are voxels of interest where the desire tract is set to start.

Users can choose voxels to be set as these starting points as well as mid and end points. A tract will then start at this seed point and follow the principal eigenvector direction to the next adjacent voxel, until the terminal voxel (Figure 2.6). However, this method is unable to account for inherent uncertainty in estimates of fiber orientations[69] and is susceptible to noise.

Probabilistic Tractography, in contrast, provides a probability distribution of fiber orientations for each voxel. This type of methods are more computationally expensive, but concede the estimation of uncertainty in the trajectory of a given tract, making it possible to determine the likelihood of a streamline to propagate in any particular direction[70] (Figure 2.7). With these techniques, one can infer global fiber trajectories.

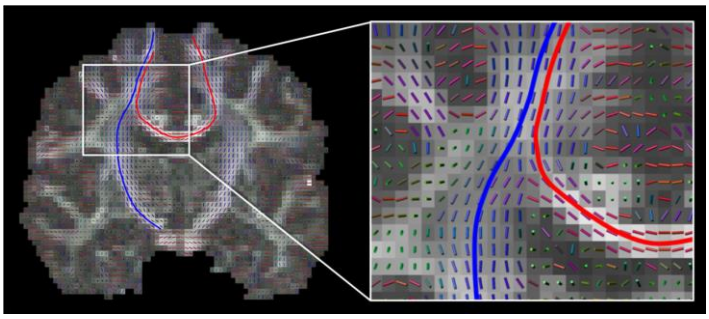

Figure 2.6 *- Vector field of local predominant fiber orientations (deterministic tractography) and two of its streamlines depicted on a coronal view of the human brain*[66].

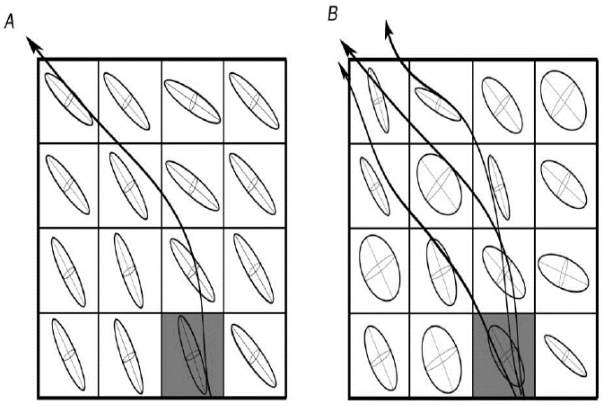

Figure 2.7 *- Visual representation of the differences between deterministic (A) and probabilistic (B) approaches to tractography. Probabilistic approaches are considerably more extensive and computationally demanding, as they track all orientations in all voxels adjacent to the seed point (grey)*[68].

Several studies[66,71] suggest that in order to understand how the brain operates as a whole, not only do we need to understand which cortical regions are active, but it is also important to map out the physical connections that mediate information transfer between the regions. Thus, this ability to describe white matter fiber pathways of the brain non-invasively offers enormous potential for the study of brain anatomy and function, as well as raising new possibilities for clinical applications.

2.3.1. DTI and CSD-based tractography

There are some disadvantages concerning streamline count and diffusion-based measures of axonal structure. One primary problem is that these measures are normally sensitive to factors such as axonal number, density, caliber, or myelination, that are not necessarily related with meaningful characteristics of anatomical connectivity strength. These tissue properties can be problematic in the interpretation of connection weights derived from diffusion MRI due to complex fiber geometries within a voxel, changes in the signal-to-noise of different voxels due to head motion, or other imaging artifacts[70]. For example, crossing fibers within a voxel have important implications for tractography in particular, as the proportion of multiple fibers within WM voxels in the brain has been demonstrated to be at least 90%[72].

The problem with diffusion tensor it that it is only capable of distinguishing a single fiber population per voxel (see Fig. 2.8) and it is often a poor representation of the underlying fiber orientations with complex architecture. Consequently, it can cause false negatives, in which tracking can terminate prematurely[73,74], or false positives, in which tracking can switch to an unrelated adjacent tract[74,75]. Therefore, a further problem regarding DTI-based tractography is the difficulty on reconstructing long-range pathways because they present streamlines with more opportunities to deviate from the normal course and are thus the most challenging to accurately reconstruct[70], which hinders the investigation of structural brain connectivity.

Recently, more sophisticated methods such as Constrained Spherical Deconvolution (CSD), introduced by Tournier and colleagues[76], have been developed in order to estimate the full fiber orientation distribution function (fODF)[77]. CSD aims at modeling the actual fODF, rather than water displacement. The fODF reflects the actual orientations of distinct fiber populations by modeling complex fiber configurations as linear combinations of Dirac's delta functions[77]. As the major limitation of DTI-based tractography is the inability to correctly describe complex fiber configurations such as crossing fibers, CSD seems a better option to optimize this technique (Figures 2.8 and 2.9).

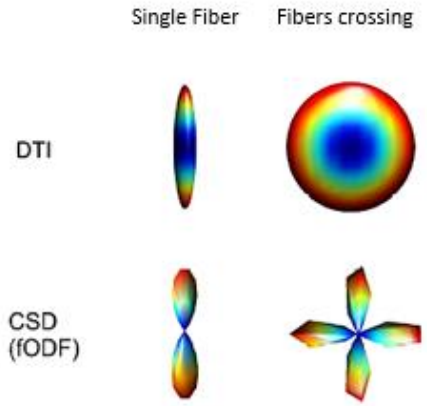

Figure 2.8 *- Example of three-dimensional (3D) profiles obtained using DTI and CSD methods in the case of single fiber configuration and two fibers crossing at 90º. When using DTI, the single fiber case is reconstructed accurately. When two fibers are crossing, it loses the possibility to discriminate the two main orientations. However, CSD reconstructs the 3D orientation distribution functions more accurately. Regarding fibers crossing, CDS technique is very precise.*

This allows for tractography to continue through regions with complex fiber configurations[74], and takes into account more than one direction per voxel, which enables a more accurate investigation of structural connectivity in vivo[23] (see Figure 2.9).

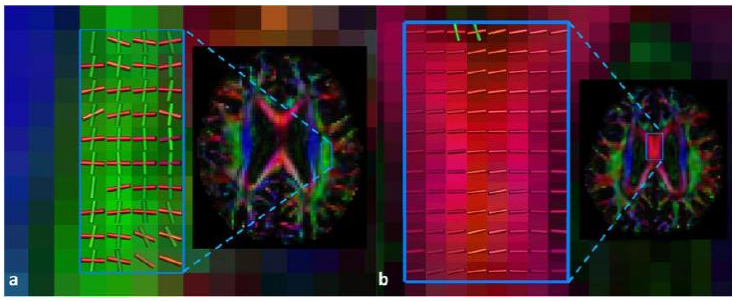

Figure 2.9 *- Fiber orientation distribution profiles estimated with the CSD method. a) two crossing fiber populations in voxels in the superior longitudinal fasciculus. b) one fiber population in the corpus callosum. Image from Reijmer, Y. D.* et al. *2012* [78].

The majority of tractography studies still employ DTI-based tractography lacking the ability to recognize complex fiber configurations. Only a few studies[23,78] have already specifically used CSD-based tractography for investigating the reproducibility of different brain network metrics, connectivity weights or reconstruction parameters.

CSD-based tractography reconstruction is slowly becoming one of the more popular strategies to investigate brain connectivity, since it has been developed to mitigate the adverse effects of ‘‘crossing fibers’’ on DTI based FT[78].

2.4. Diffusion-Based Connectomics

In 2005, the term Connectome was simultaneously suggested by Sporns and Hagmann, to refer to a map of the neural connections within the brain[79,80]. Since then, "Connectomics", also known as brain network analysis, has been defined as the science concerned with assembling and analyzing connectome data sets.

The whole-brain structural connectivity can then be modeled as a network with diffusion-MRI and tractography, to study the white-matter fibers connecting brain areas. Tractography can reveal the trajectories of white matter pathways in vivo and infer the underlying structural connectome of the human brain. As the connectome term refers to a brain network of connections, network **nodes** are associated with distinct grey-matter regions, while white-matter fiber bundles serve as interconnecting network **edges**. Therefore, fiber tractography claims a central role in the field of Connectomics, as it allows the study and building of comprehensive maps of the complex network of connections within the brain[66].

2.4.1. Defining Nodes

A graph is an abstract representation of a network, consisting of a set of nodes (vertices) and edges (connections). Nodes are commonly defined as populations of neurons. Nodes can also correspond to individual voxels in an MRI dataset, but often thousands of neurons confined in a single MRI voxel may contain cells from different populations[70]. In connectomics, the four most common strategies for node definition are: (1) Anatomical, based on a priori anatomical information such as sulcal and gyral landmarks; (2) Random, by defining discrete nodes of similar size based on a random parcellation of the brain; (3) Functional, by using functional information such as coordinates of peak activations; and (4) Voxel-based, where each image voxel represents a distinct node[11].

One of the most used parcellations is the Automated Anatomical Labeling (AAL)[17] which is an atlas of the human brain. The AAL atlas was constructed through the identification of major and minor sulci on a T1 MRI with subsequent labeling based on anatomical location (see Figure 2.10). It also includes the whole brain gray matter and is consistent with other that used sulci as landmarks for regions delineation[17].

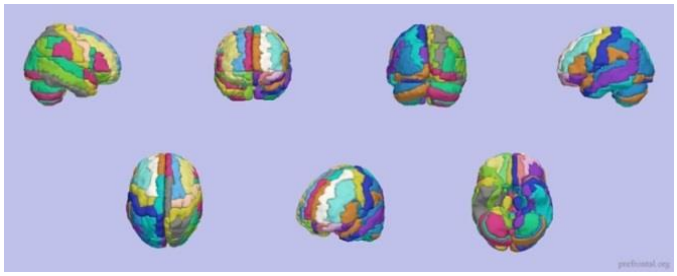

Figure 2.10 *- Automated anatomical labeling (AAL) parcellation. Image from Prefrontal Cog Neuro MRI, Brain Art: AAL Patchwork, 2008, accessed 28 November, <http://prefrontal.org/blog/2008/05/brain-art-aal-patchwork/>.*

2.4.2. Defining Edges

Described as the connections between nodes, edges can be defined by different types of connectivity: Direction, Weigh and Heterogeneity. Directed edges denote that each anatomical connection emerges from a source region and links to a target, whilst undirected edges only have the information about the existence of the connection, yet the direction is unknown. Weighted edges assume that the connections between regions vary (i.e., are weighted) according to the strength of their interaction. Lastly, heterogeneity distinguishes regions that make different types of connections (e.g, excitatory, inhibitory, modulatory) with other parts of the brain[11].

A matrix that represents the connections between brain regions is a **directed graph** or network if the element C_{ij} does not necessarily have the same value as the element C_{ji}, and the matrix is asymmetric (Figure 2.11-A and 2.11-B). These matrices allow us to map the influence that on node has on another. Different authors have different ways of representing the directionality, and sometimes, efferent projections are listed down the columns and afferent projections along the rows, or reversed, and this must be precisely indicated. For example, as depicted in Figure 2.11-A and 2.11-B, the element $C_{F,C}$

encodes the edge projecting from node *C* to *F*, as illustrated on the graphs above the matrices. Figure 2.11-A corresponds to directed graph, with directionality represented using arrowheads (upper panel), as well as a **weighted graph**, as connection strengths are represented as variations in edge thickness of the arrows. The corresponding connectivity matrix (lower panel) uses colors to represent variations in edge weights. The corresponding **unweighted graph** is presented in Figure 2.11-B, where all edges have the same thickness (upper panel), and all connectivity weights of the matrix (lower panel) have a value of zero or one, indicating the absence or presence of a connection.

In contrast, if the connectivity matrix has identical upper and lower triangles, we have $C_{ij} = C_{ji}$. This means that the matrix represents an **undirected graph**. This type of networks allows us to identify which connections exist between specific pair of network nodes, but do not give information about the directions of those connections. An example of an undirected graph is shown in Figure 2.11-C and 2.11-D. Arrowheads are no longer required in the graph representation (upper panel) as there is no directionality, and upper and lower triangles of the connectivity matrix (lower panel) are mirror images of each other.

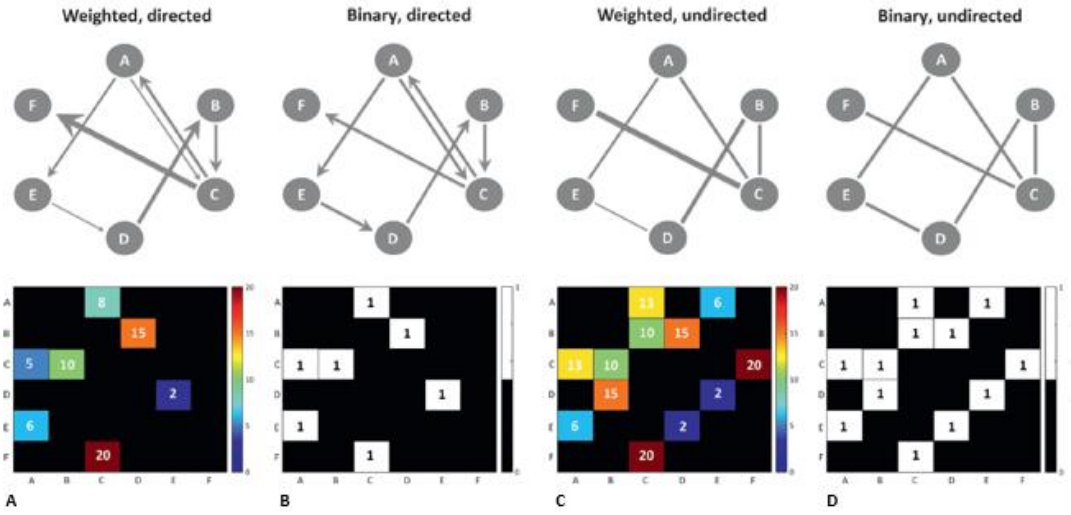

Figure 2.11 *- The equivalence between graphs and matrices.* ***(A)*** *A weighted, directed network graph (upper panel) and its corresponding connectivity matrix (lower panel).* ***(B)*** *A binarized or unweighted version of the directed network depicted in (A).* ***(C)*** *An undirected version of the weighted network depicted in (A). The corresponding adjacency matrix is symmetric, such that Cij = Cji.* ***(D)*** *A binarized and undirected version of the network in (C).*
Image from the book of Fornito et al. [70].

2.5. Brain Network Analysis

In 2009, Bullmore and Sporns suggested that a brain network study involves the following four steps[81] :

• Defining the network nodes by subdividing the cortex into several brain regions. This can be achieved by performing fine parcellation or atlas based parcellation, such as the Automated Anatomical Labeling (AAL) atlas[15,17].

• Estimate the edges, as a measure of association between nodes. For example, the fiber tracts generated with DTI that connect a pair of regions.

• Create an association matrix by compiling all pairwise associations between nodes and (usually) apply a threshold to each element of the matrix to produce a binary adjacency matrix or a brain graph.

• Use graph theory to calculate the network parameters of interest in this graph theoretical model of a brain network and compare them to the equivalent parameters of a population of random networks.

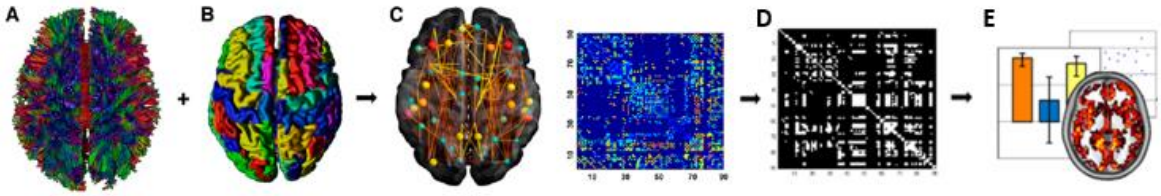

***Figure 2.12** - Flow chart of constructing a diffusion weighted imaging-based network: (A) With a whole-brain fiber tract reconstruction and a subcortical brain regions parcellation (B) is possible to obtain a brain network and its representation by a connectivity matrix (C). The application of an threshold creates a binary matrix (D), which can be used to study some brain properties (E). Image adapted from the work of Reijmer* et al.[82] *and Telesford*[83].

Many existing studies in the broader literature[15,70,84] have followed this pipeline to analyze brain networks (Figure 2.12). Brain imaging data are first processed and analyzed to produce a matrix that denotes the strength of connection between nodes. This matrix then offers a compact description of the pairwise connectivity between all nodes of a network. Then, a threshold is commonly applied to the matrix to generate a binary adjacency matrix, where the weights associated with the remaining edges are omitted, leaving only information about whether edges are absent (0 in connectivity matrix) or present (1 in connectivity matrix). From this binary matrix, various graph metric analyses can be performed. Both weighted and binary connectivity matrices can be used to apply graph theory to study and analyze the connectivity matrices.

2.5.1. Graph Theory and Graph Measures

The field of graph theory was propelled forward when Watts and Strogatz[85] introduced their small-world network model, which described a network that provided regional specialization with efficient global information transfer[15]. Once nodes and edges are accurately defined, graph theory can be used to

characterize a wide array of network properties. This kind of approach has gained popularity in the past decades because it seems to provide an adequate, yet simple model of a complex system as the brain[86]. When used thoughtfully, these methods can provide novel insights into brain organization[11] as graph topology can be quantitatively described by a wide variety of measures. In studies of clinical and technical neuroscience, complex network theory is particularly appealing as many emotional and cognitive disorders have been already characterized as dysconnectivity syndromes. This is due to the presence of unusual phenotypic profiles of anatomical/functional connectivity between brain regions[87], concluding that disconnection leads to dysfunction[88].

It is possible to study a wide range of graph measures. The **degree of a node** is defined as the number of edges connecting that node to the rest of the brain graph (Figure 2.13-A), and **degree centrality** has been used to discriminate between nodes in the system that are well connected, i.e., so-called **hubs**, and nodes that are less well connected, or nonhubs (Figure 2.13-C). The indicators of centrality identify the most influential nodes within a network. In a social network, it is used to identify the most influential person[87]. Regarding brain networks, a hub is a regional node with high centrality that plays an important role in the dynamics of the system, as it is involved in many of the shortest paths between other regions of the whole brain network[89]. For a weighted graph, **node strength** represents the sum of weighted edges to the node.

The Watts–Strogatz small-world model (1998) introduces two other important measures: clustering coefficient and characteristic path length[85]. The **clustering coefficient** is a measurement of the efficiency of local connectivity[89] and quantifies the number of connections that exist between the nearest neighbours of a node as a proportion of the maximum number of possible connections. Moreover, if the nearest neighbors of a node are also directly connected to each other they form a cluster (Figure 2.13-B)[81]. The characteristic **path length** is the average of the minimum number of edges required to link any two nodes in the network (Figure 2.13-D)[87]. A related and often more sensitive measure is **betweenness centrality**, defined as the fraction of all shortest paths in the network that pass through a given node[90]. Path length is commonly used to determine the global efficiency of information transfer within a network[86]. **Global efficiency** is defined as the average of efficiency for all node pairs, as it is a measure of parallel information processing ability[82]. A network with high global efficiency will have a short characteristic path length and will be more optimized as a cognitive workspace[89].

These last two metrics also enable us to define the **small-world** property, as the combination of high clustering and short characteristic path length[89], since shorter average path length results in more rapid and efficient integration across a network[87]. The "small-world" phenomenon is based on real-world networks[85,91], describing the simultaneous presence of locally clustered connectivity and short path lengths between regions. This network organization provides a topological basis for the dual properties of functional segregation and functional integration, are key principles of the organization of the brain[92,93].

Finally, **modularity** is a measure that describes the fact that many networks are divided in modules (Figure 2.13-E). Each module contains several densely interconnected nodes, and there are relatively few connections between nodes in different modules. Connector hubs are nodes that make the connection between modules[94]. Mathematical definitions of these network measures can be found in the Appendix.

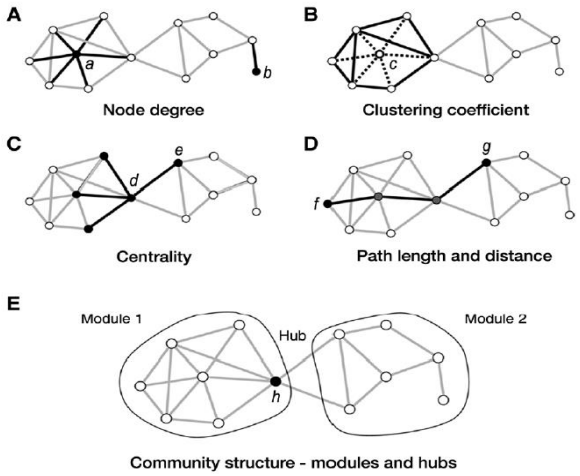

Figure 2.13 *- Representation of the basic network properties. The measures are illustrated with a simple undirected graph with 12 nodes and 23 edges.* ***(A)*** *Node degree. The node a has a degree of 6, and the peripheral node b has the degree of 1.* ***(B)*** *Clustering coefficient. In this example, the central node c has 6 neighbors, and these neighbors maintain 8 out of 14 possible edges. Thus, the clustering coefficient is 0.57 (8 of 14).* ***(C)*** *Centrality. In this example, node d contributes more to the centrality because all nodes on the right-side pass through the node d to reach the other nodes in the left side.* ***(D)*** *Path length. The shortest path length between the nodes f and g is three steps that pass through two intermediate nodes.* ***(E)*** *Modularity. In the example, the network forms two modules interconnected by the single hub node h. Image from the paper of Sporns*[95].

A study by Tuladhar *et al*. (2016), found that SVD-severity (indicated by higher WMH load, number of lacunes and microbleeds, and lower total brain volume) was related to networks with lower density, connection strengths, and network efficiency, and consequently to lower scores on cognitive performance[41]. The study also explains the importance of network analysis in the understanding of SVD-related cognitive impairment in addition to conventional MRI markers for SVD, suggesting that it might provide a useful tool as disease marker.

Other reports show that disease related changes in topological properties of brain graphs can be related to other aspects of the disorder in question. For example, reductions in network efficiency have been associated with greater white matter lesion load in 330 patients with multiple sclerosis[96], and reductions in nodal efficiency have been associated with greater severity of local amyloid deposition in patients with Alzheimer's disease, as shown in a study by Buckner *et al*.[97]. This study, with 127 participants, shows the importance of hubs in brain networks, as it explains that high amyloid-deposition in the locations of cortical hubs, while acting as critical regions for information processing, may also augment the underlying pathological cascade in AD.

In a study by Reijmer *et al*.[2], they constructed the structural network of fifty patients with mild cognitive impairment (MCI) or dementia and examined correlations between measures of local and global network connectivity and cognitive performance on several cognitive domains. Secondly, they examined whether network parameters can provide information that is complementary to abnormalities visible on conventional MRI (i.e., cerebral atrophy and SVD). The results showed that a less efficient organization of the WM network is related to worse memory and executive functioning. Additionally, measures of network efficiency explained a substantial proportion of the variance in cognitive functioning on top of

markers of brain atrophy and SVD, indicating that network measures provide information that is clearly complementary to widely used conventional MRI biomarkers.

Graph theory thus provides a common language for the analysis of complex systems in general, and allows the description of the key topological properties of nervous systems from the cellular scale of the neuronal connectome[89], to the whole-brain scale of human neuroimaging data.

However, despite the potential of network analysis and to quantify topological modifications, the methodology is significantly vulnerable regarding the comparison of networks with different densities and degree distributions[11,18]. This is due to the topological metrics being highly dependent on the network density[98].

2.5.2. Thresholding Problem

Due to the noisy and indirect measurement of water diffusion combined with the nature of probabilistic tractography, the resulting structural brain networks are known to contain a substantial percentage of spurious connections[10,70,86]. Therefore, network thresholding methods are widely used to remove spurious connections, but it is not yet clear how different thresholding strategies affect basic network properties[21]. Some network studies have employed thresholding strategies, such as, **absolute-thresholding** which applies a uniform threshold to retain only connections above a set weight[6] and **density-thresholding** which applies a relative threshold (Figure 2.14) on the connection weights such that the weakest connections are remove to match the same number of connections across subjects[90]. This last type of thresholding tries to remove the effect of **network density** on graph measures[18,98], that is defined by the percentage of connections available (i.e. the number of detected edges divided by the number of all possible edges).
Buchanan *et al.* (2019), explains that network thresholding methods are already widely used to remove ostensibly false connections, however, is not yet clear how different thresholding strategies affect basic network properties, or whether crucial connections can be incorrectly removed[21]. A study by de Brito Robalo *et al.* (2020), suggests that fixed-density thresholding might improve the detection of between-group differences[99].

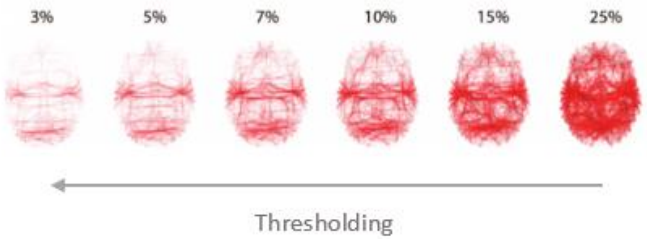

Figure 2.14 *- Thresholding process regarding brain network (percentage numbers refer to the density value on each point of thresholding process).Thresholding increases to the left, causing the density to decrease.*

However, although brain connectivity graphs are being used to study the properties and evolution of some diseases, the clinical differences in brain graphs can be challenging to interpret. This is mainly due to the complex patterns of adaptive responses, as well as the progressive nature of connectivity deficits in many brain diseases. Moreover, analysis of brain graphs in clinical populations requires care in the

attribution of biological meaning to some network measures, that is based on many assumptions. For example, in a brain graph, path length measures assume that neural information is transmitted via the shortest paths[70,100], as they allow more direct transmission of neural signals[101], however this remains to be established so that these models based on diffusion processes may be considered reasonable[84].

The choice of a threshold plays an important role in network analysis, as it affects the density of connections and impacts network topology. It would be argued that thresholding can mask true group differences or introduce artificial group differences that are not present in the first place. Network thresholding presents a difficult challenge, as there is no consensus on what strategy to use. Within the literature, it is common to show how graph metrics change over various thresholds[18,25,102].

Proposed normalization procedures to correct for these biases in both unweighted and weighted network analyses do not provide an equate solution. Normalization typically involves comparison of estimated network characteristic to those for reference network with the same density, and sometimes also the same degree distribution. A study by van Wijk *et al.* (2010), shows that this normalization step may reduce the bias but does not solve it completely, as it introduces other bias that were absent before[18].

Therefore, due to the lack of rules about how these networks should be reconstructed, there is no gold standard model of the human brain network yet. Adding this to the fact that the diffusion MRI is a very indirect measurement, the accuracy of the fiber tractography turns out to be very dependent on methodological aspects. Consequently, networks have low reproducibility over time, and it can be difficult to distinguish real network changes only due to disease from artificial changes caused by these methodological issues.

Thus, how can we compare and study brain networks correctly?

2.5.3. Brain Network Backbones

One proposed solution to reconstruct a standard brain network model in order to create a reliable and robust method for comparison is found in the literature[10,24,103]. The idea is to perform network analysis using a backbone of the network instead of the whole-brain network. This backbone should be a structure with strong connections over which the network is built on. The aim is to build a network to reduce the noise due to methodological issues, while keeping the main characteristics of the network and still being a reliable way to detect disease-related changes. Increasing evidence suggests that structural brain networks, particularly their backbone, are altered in neurological and psychiatric disorders, and heterogeneity in these alterations is evident between diseases[81,94,98]. It is of clinical interest that many of these network changes (in clustering and path length) and connectivity loss, are associated with cognitive deficits and behavioural changes[2,104–108].

Therefore, a reference network could serve as a null-model to characterize network alterations in individual subjects[10], and to develop theoretical models of altered connectivity patterns during maturation or due to disease[11]. Although this concept is still quite new, from literature review we found that are 4 main concepts of backbones that had already been proposed: Minimum Spanning Tree[10,20], Disparity Core[24], K-Core[28] and Hub-Core[16]. Excluding the Disparity Core, all the others have already

been applied to the study of the brain. Nevertheless, there is a lack of a reference for the human brain network even if scanning and preprocessing conditions remain unchanged[11,26].

Minimum Spanning Tree (MST) is a backbone based on the Kruskal algorithm[109], that ensures that every node is linked to the rest of the network without forming loops, comprising the strongest connections. In graph theory, a tree is a undirected graph in which any two vertices are connected by exactly one path or, equivalently, a connected acyclic undirected graph[110]. This facilitates network comparisons without normalization or standardization steps[13]. The usefulness of the MST method has been proved in weighted network studies[20,111], aging alterations in connectivity brain studies[13,112] and in the comparison of healthy and diseased groups, in capturing subtle developmental brain network changes[26,113].

Disparity Core, introduced by Serrano *et al.* in 2009, or multiscale backbone, is a particular technique that operates at all the scales defined by the weighted network structure. The disparity filter proceeds by identifying which links for each node should be preserved in the network. This method is based on the local identification of the statistically relevant weight heterogeneities. The algorithm can sufficiently reduce the network without destroying the multi-scale nature of the network, by filtering out the backbone of dominant connections in weighted networks with strong disorder and preserving structural properties and hierarchies at all scales.

The K-core decomposition consists in identifying particular sub-graphs, called k-cores. This is done by identifying subsets of graphs by recursively removing all the vertices of degree smaller than k, until the degree of all remaining vertices is larger than or equal to k[27,28]. Vertices with larger degree and more central position in the structure of the network, correspond to larger values of the index k.

Finally, the Hub-Core is defined by high-centrality nodes, called Hubs. It has been noted that some of these hubs play a central role in the overall network organization, as indexed by a high degree, low clustering, short path length, high centrality and participation in multiple communities across the network[114]. In addition to being individually highly connected ("rich"), brain hubs exhibit a strong tendency to link to each other, forming a structural core or Rich-Club[16]. A rich club is defined as a subset of nodes with high-centrality, maintaining a large number of connections across the network (i.e., high degree), and their tendency, as the dominant elements of the system, to form a tightly interconnected community[115], establishing more links among themselves than randomly expected[116]. This sub-network uses the strongest network hubs, maintaining their connections while removing weaker ones, used to test the preservation of hub locations[103].

In a study by van Dellen *et al.* (2018)[10], MST was used as an empirical reference network in order to form the backbone structure of the human brain, and the results show that MST provides an elegant and straightforward approach to analyze structural brain networks, and to test network topological features of individual subjects in comparison to empirical null models. However, since the MST only contains a small fraction of the original network (Figure 2.15), it becomes difficult to study the network at a local level. Nevertheless, recent studies[13,112,113] have shown that MST analysis can be used to capture network alterations due to aging and disease in both functional and structural imaging data.

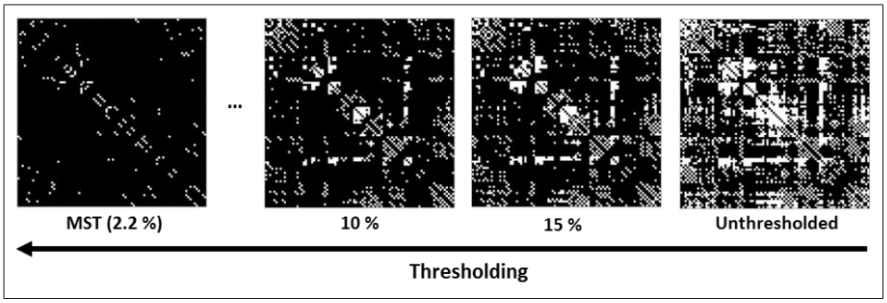

Figure 2.15 - *Thresholding process regarding the adjacency matrix. The un-thresholded image represents the binary matrix before the application of any threshold. MST method is computed with a network density of 2.2%. See section 3.1.5. for backbone reconstruction.*

Some other papers suggest[81,98] that structural brain networks, particularly their backbone, are altered in neurological disorders, and heterogeneity in these alterations is evident between diseases[10]. However, no study has investigated if these backbones are reproducible over time (in scan-rescan scenarios) or if they can be used to study disease effects in clinical populations.

3. Methods

3.1. DATASET

3.1.1. Participants

Patients included in this study were 87 individuals from the Parelsnoer study[29]. Patients who were referred to the memory-clinic of the UMC Utrecht for evaluation of cognitive problems, with a clinical dementia rating scale (CDR)[117] score of 0, 0.5, or 1, and a Mini-Mental State Examination (MMSE)[118] 20 or higher were eligible for the study. Patients were eligible for the current analysis if they had an MRI-DTI scan at baseline and after ~2 years follow up visit date (N=90). We additionally excluded three patients with cognitive complaints due to a diagnosis other than SVD or Alzheimer's disease (AD). Thus, the total number of subjects included in the analysis was 87 (59 % male). These patients had an average age of 72 +/- 7 years, scanned twice with and inter-scan time between baseline and follow-up of 27 +/- 4 months. From these patients, 53% were diagnosed with MCI, 36% with dementia, and most of them had some form of SVD injury, presence of lacunes and microbleeds.

In addition, 45 age- and education-matched elderly without dementia or other known neurological disorder that could affect cognition, and a MMSE score between 28 and 30, were included as a control group. Control participants were recruited from Utrecht Diabetic Encephalopathy Study (UDES)[31] study, with DTI data only from baseline.

A Validation data group was also included in the study, consisting of high-quality scans of healthy young adults, to test the effects of network backbones on a 'clean' dataset without the presence of disease effects. These scans were obtained from the Human Connectome Project[30]. We included 44 healthy participants (32% male) with a test-retest DWI and T1-weighted images. The interval between the two scans ranged between 5.5 +/- 4 months, and the age of the participants varied between 22 and 35 years old. As the age of the validation dataset did not match the Patients, their data was only used to examine whether the same pattern of network backbone reproducibility could be found between these two datasets. This validation data was not used to operate as controls for the longitudinal disease-progression analysis. Characteristics of the study population are given in Table 3.1.

3.1.2. MRI acquisition

MRI data of patients and UDES controls were acquired on a 3 tesla Philips scanner (Achieva, Philips, Best, the Netherlands) using a standardized protocol that included a 3D T1-weighted image and a diffusion weighted sequence. T1-weighted scans were acquired with the following parameters: isotropic acquisition voxel size of $1mm^3$, a flip angle of 8º, echo time (TE): 4,5 ms and repetition time (TR):7,9 ms. DWI scans had an isotropic acquisition voxel size of 2.50 mm3, 45 diffusion-sensitizing gradients with a *b-value* of 1200 s/mm^2, and 1 b=0 s/mm^2.

***Table 3.1 - C**haracteristics of the study population. Data presented as mean ± SD, absolute number (percentages) or median [interquartile range]. Abbreviations: MMSE = Mini Mental State Examination; ICV = Intracranial volume; WMH = White matter hyperintensities; SVD = Small Vessel Disease.*

	Patients with SVD N=87 (two time-points)	Controls N=45 (one time-point)	Validation data N=44 (two time-points)
Demographic Characteristics			
Baseline age, in years	72.6 ± 7.5	72.0 ± 4.6	31 ± 4
Sex, female	41%	47%	68%
MMSE	26 [20-30]	29 [28,30]	-
Imaging markers			
Fazekas score (0-3)	1 (0-3)	-	
WMH volume (%ICV)	1.1 [0.4,2.2]	0.4 [0.2,0.8]	
Lacunes (present)	31 (36%)	2 (4%)	
Microbleeds (present)	18 (21%)	-	

Validation data scans were acquired on a Siemens Skyra 3 tesla scanner (Siemens, Erlangen, Germany). The T1-weighted images had an isotropic voxel size of 1.25 mm^3. The multi-shell DWI were acquired with an isotropic voxel size of 1.25 mm^3 and three diffusion weightings (b-values: 1000, 2000 and 3000 s/mm^2). For each b-value, 90 diffusion-sensitizing gradients directions were measured. Additionally, 18 images with no diffusion weighting (b-values = 0 s/mm^2) were obtained. Here, we selected only a single shell (b-value 1000 s/mm^2) since it was more comparable to the patient dataset described above. Furthermore, a fluid-attenuated inversion recovery sequence (FLAIR; TR/TE/Inversion time = 1,000 /125/2800ms) was acquired to rate neuroimaging markers of SVD (i.e., brain volumes, WMH volume, and lacunes) (Table 3.1).

3.1.3. Image Processing

Diffusion-weighted data were processed using ExploreDTI[119], running on MATLAB R2014b (MATLAB and Statistics Toolbox Release 2014b; The MathWorks, Inc., Natick, MA). Data were corrected for signal drift, subject motion, eddy current, and susceptibility artifacts, including rotation of the B-matrix before the estimation of the diffusion tensors. The diffusion tensors were computed using robust estimators[120] followed by whole brain tractography. Then, the tractography model was created. Each streamline was propagated using integration over fiber orientation distributions (FODs). Streamlines were guided by fiber orientations inferred using CSD with a maximum harmonic order of 6. Streamlines were terminated when they entered a voxel with FOD<0.1, or when the deflection angle between two successive steps was >45º. These tractography parameters were chosen according to recommendations from the previous literature[66].

3.1.5. Network reconstruction

The T1-weighted data were pre-processed using SPM tool CAT12. The pipeline, as illustrated in Figure 3.3, included brain extraction and parcellation of the gray matter volume into 90 cortical and subcortical regions of interest (ROIs), using the automated anatomical labeling (AAL) template[17]. The parcellation was performed in the native space, with the AAL template being warped to the T1 image of each subject[121]. The cerebellum was excluded from the analysis since most subjects had insufficient scan coverage of this structure.

For network definition, each ROI represented a node in the network. Two nodes were considered to be connected if they contained the end-points of at least one streamline, resulting in a 90 × 90 binary connectivity matrix. We also obtained weighted connectivity matrices for each subject, in which the previously defined edges were weighted by several diffusion properties, as explained in the next section.

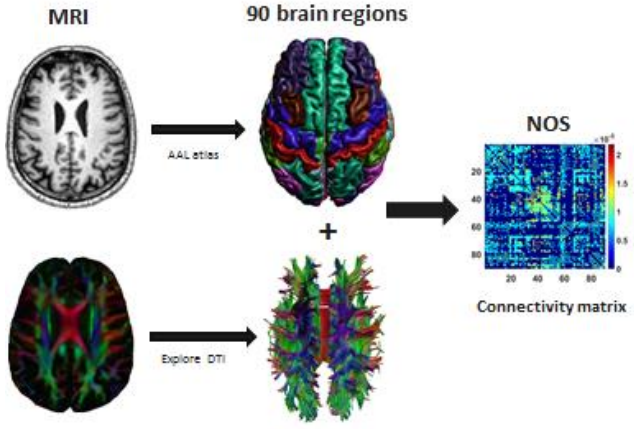

Figure 3.1 *- Flowchart of the structural network reconstruction.*

3.1.4. Testing weighted network reproducibility

Before proceeding to our main analysis, we investigated which network weight should be the best one to test reproducibility and to compare disease progression over time and between cohorts. The node degree, i.e. the number of edges that each node has, also called Number of Streamlines (NOS), is frequently used in this approach. The NOS-weighted matrix is typically used for thresholding. However, since there is no consensus on which DTI property provides the best representation of the structural brain network, we examined several weighted networks, based on average FA, average MD, variance of FA-variance and variance of MD.

In the connectivity matrix, due to the indirect nature of diffusion measurements, some voxels might contain extreme values of FA and MD (e.g. very close to 1 or 0), which is not plausible in true white matter. Thus, when we define the weight of a connection based on the mean FA or mean MD of that fiber bundle, it is likely to be affected by these methodological issues.

Similar to the peak skeletonized mean diffusivity measure by Baykara et al.[4], we propose the same approach but regarding also FA measures. First, we compute the histogram of FA values of all voxels connecting the pair of ROIs. Then we take the difference between the 95th and 5th percentile of the histogram peak. Finally, we create FA and MD variance matrices based on the "edge-homogeneity" measure, where each element represents how homogeneous and robust a connection is. Note that the higher the variance, the lower the edge homogeneity.

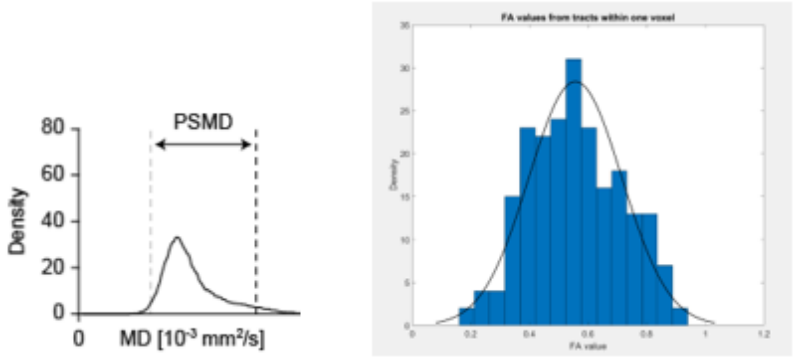

Figure 3.2 *- On the left is the histogram from Baykara* et al.[4]*, to analyze mean diffusivity (MD) data, with calculation of the Peak width of Skeletonized Mean diffusivity (PSMD). On the right is our example of all FA values within a voxel from one subject that is, as expected, a normal distribution.*

We compared the reproducibility of the network weights (NOS/FA/MD/FA and MD variance) matrices, only on the common nodes between both time-points. We used Pearson Correlation to obtain the results for the reproducibility between both time-points. The boxplots presented in Figure 3.2 highlight that the best network weight to study reproducibility is the Number of Streamlines. Therefore, for the following analysis, we used the NOS as the network weight.

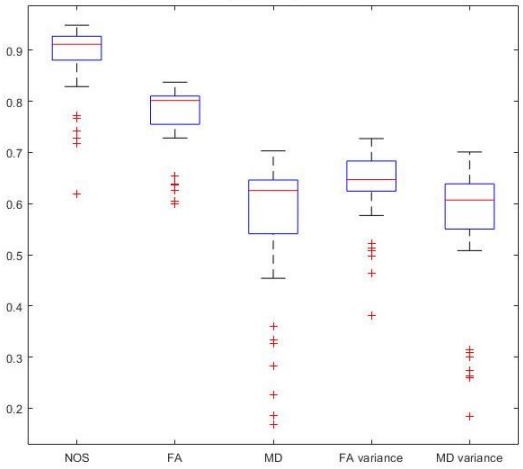

Figure 3.3 – *Reproducibility values between time-point 1 and time-point 2, regarding different network weights. The first boxplot concerns the reproducibility of the network regarding the number of streamlines. The second and third are related to the FA and MD weighted networks reproducibility. The last two are related to the FA variance and MD variance network weights.*

3.1.5. Backbone reconstruction

To reconstruct each backbone, we applied a specific algorithm to the NOS-connectivity matrix of the whole-brain network (Figure 3.4). We therefore used 4 backbones: Minimum spanning Tree (MST), Disparity-Core, K-Core and Hub-Core (Figure 3.5).

Each backbone algorithm was based on the literature. Regarding MST, as it is a sub-network of the original weighted network that connects all nodes in the network without forming loops, MSTs are constructed based on the weighted networks with Kruskal's algorithm. In our case, based on the paper by Tewarie et al.[20], we started the algorithm with the largest edge weights since we are interested in the strongest connections in the network. This algorithm first sorts the weights of all edges in a descending order and starts the construction of the minimum spanning tree with the largest edge weight and adds the following largest edge weights until all nodes N are connected in an acyclic sub-network that consists of M=N−1 connections, i.e. a fixed density. If the addiction of an edge forms a loop, this edge is ignored. After construction of the MST, all link weights are assigned a value of one, creating a binary matrix, as shown in the scheme of Figure 3.4.

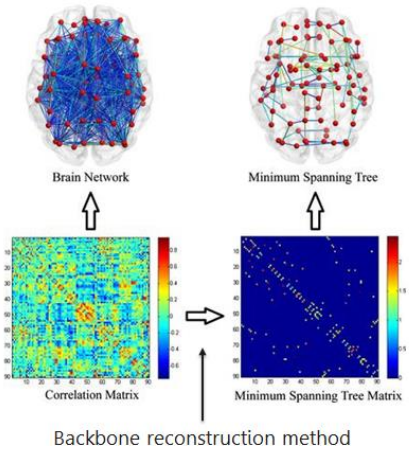

Figure 3.4 *- Backbone matrix creation. From the original connectivity matrix, a backbone reconstruction method is applied to obtain the backbone matrix.*

K-core decomposition reduces a graph into a maximal connected subgraph of nodes with a minimum degree of k. Therefore, to compute the "18-core" (for example) of the connectivity matrix, all nodes that have a degree 18 or higher are retained; nodes that do not satisfy this condition are removed. Thus, in this example, 18 represents an arbitrary cut-off (k-value) to define which nodes will constitute the backbone. For this study, we defined our k-value for the K-Core backbone, based on the first quartile of the degree distribution. Thus, the k-value varies for each individual, but it is always based on this condition. The quartile vector of the degree distribution of some connectivity matrix is, for example: [16,22,28]. And in this case, we would use the 16-core to threshold the matrix in order to construct the k-core backbone. These are the steps to construct the K-Core backbone, for a particular sum of weights k:

1. Remove all nodes of degree <k, resulting in a reduced connectivity matrix M'.

2. From the remaining set of nodes, compute the connectivity strength k for each node. If nodes are found that have a lower level of connectivity than k, step 1 is repeated to obtain a new M'; otherwise, proceed to step 3.
3. The remaining subset of nodes forms the k-core of the network.

The disparity core identifies which edges for each node should be preserved in the network. Firstly, we calculated the betweenness centrality[122] (BC) of the connectivity matrix (see Appendix for further information), which is the fraction of all shortest paths in the network that contain a given edge. Thus, edges with high betweenness centrality participate in a large number of shortest paths.

Regarding the Hub-Core, in order to preserve the hub locations[103], the algorithm aims to find a sub-network composed by the strongest network hubs, maintaining their connections while removing weaker ones. To build this backbone, we followed these steps:

1. Calculation of the betweenness centrality and the degree (D) for each node, resulting in a matrix with the Hubscore (HS) value of each node, where HS = BC x D.
2. Were considered Hubs all nodes that had the HS values higher than the average plus standard deviation of the total Hubscores. HS > average (HS) + SD (HS).
3. Those hubs and their connections were used to build the backbone.

In Figure 3.5 are shown the different backbones built with 90-nodes AAL template, and the original network. As we see, they are all very different between them, and have distinct particularities.

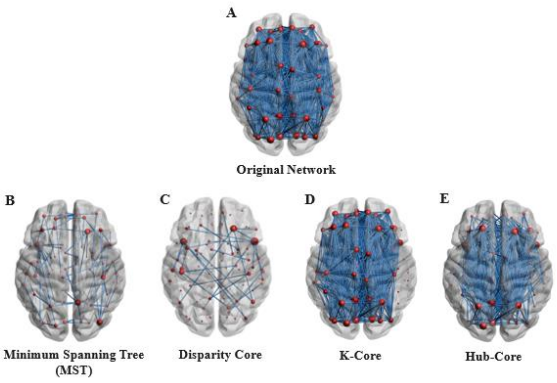

Figure 3.5 - *Network backbones used for the analysis using a 90-node template.*

3.1.6. 200-node and 250-node templates

We also wanted to look at other brain templates to understand whether the choice of parcellation scheme could affect the results of our backbone analysis. Thus, we performed the same analysis with a 200-nodes whole-brain parcellation and a 250-nodes left hemisphere parcellation based on a study by Schaefer *et al*[32]., used only for the validation data at baseline. Figure 3.6 presents the network backbones reconstructed with the whole-brain 200-nodes template, and figure 3.7 shows the same network backbones reconstructed with the left hemisphere 250-nodes template. Shown in Table 3.2 are the number of nodes and edges from the average group backbone (see Section 3.2.2.) of each template.

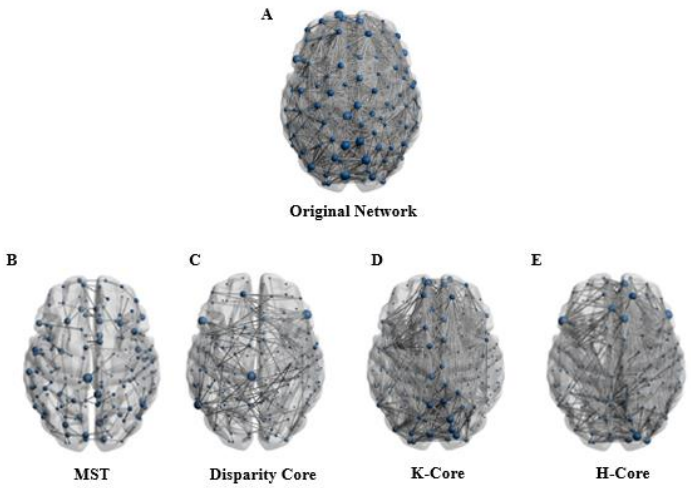

Figure 3.6 *- Network backbones used for the analysis using a 200-node template*

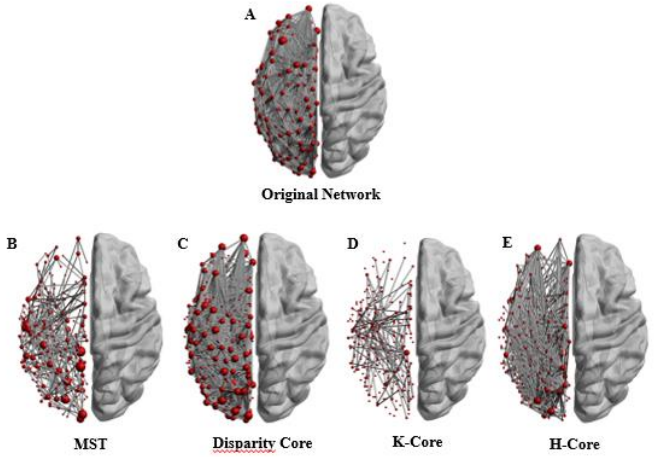

Figure 3.7 *- Network backbones used for the analysis using a 250-node template of the left hemisphere.*

Table 3.2 *- Number of nodes and connections regarding the group average backbone of each brain network, from Validation data at baseline.*

	90-node template		**200-node template**		**250-node template (left hemisphere)**	
	Nr. of nodes	Nr. of edges	Nr. of nodes	Nr. of edges	Nr. of nodes	Nr. of edges
Original network	90	30952	200	72501	250	26323
MST	90	89	200	199	250	249
Disparity Core	41	30	146	163	107	212
K-Core	49	664	94	1600	158	1724
Hub-Core	76	260	185	1103	206	565

3.2. NETWORK ANALYSIS

To analyze the backbone networks, we compared the binary backbone matrices from different time-points (within-subjects comparison), different subjects within the same group (across-subjects comparison), and between different groups (across-groups). In order to examine the structural similarity of each pair of networks, we used three approaches: whole-backbone overlap, occurrence backbone overlap and group average backbone overlap. Moreover, we also compared MST measures within subjects and across-groups.

Finally, to test sensitivity to disease effects, we compared networks between controls and patients at baseline (cross-sectional analysis), and between patients at baseline and follow-up (longitudinal analysis). For this part of the analysis, we used node strength and global efficiency

3.2.1. Network overlap

As aforementioned, the NOS-weighted matrices are transformed into unweighted backbone matrices (i.e., binary graph containing edge weights of 0 and 1 only). The similarity between backbone networks was quantified by calculating the fraction of edges present in both backbone binary matrices ranging between 0 and 1, with 0 indicating no overlap and 1 representing a complete overlap between the two sets of edges[10] (Figure 3.8). This overlap parameter was calculated as the mean between the dice overlap and a measure that we called "topology zeros overlap".

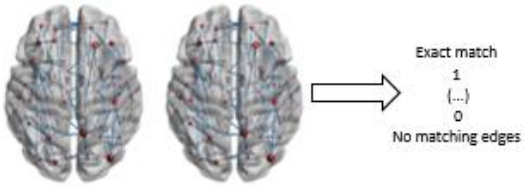

Figure 3.8 - *Schematic representation of network backbone overlap.*

The dice overlap, also called Sørensen–Dice coefficient, is a statistic parameter used to quantify the similarity of two samples. It was independently developed by the botanists Thorvald Sørensen[123] and Lee Raymond Dice[124], and given two sets X and Y, is defined as:

$$dice = \frac{2|X \cap Y|}{|X| + |Y|} \tag{3.1}$$

In this study, $|X|$ and $|Y|$ represent the number of positive edges (1 in the binary matrix) in each set, whereas $|X \cap Y|$ represent the edges in common between the two matrices. The topology zeros overlap is calculated in the same way but represents the percentage of zeros that are common in both matrices, thus $|X|$ and $|Y|$ represent the number of zeros in the binary matrix and $|X \cap Y|$ represent the zeros in common between the matrices.

3.2.2. Occurrence backbone and group average backbone

The occurrence backbone is based on the common edges of 75% of the subjects. An example with MST is shown in Figure 3.9. Firstly, we compute the MST for every subject, then we calculate the mean MST connectivity matrix of all subjects, with values that range from 0 to 1, representing frequency of that connection of all the subjects. Finally, a threshold is applied in order to keep only the values > 0.75, which means that those connections are present in at least 75% of the subjects.

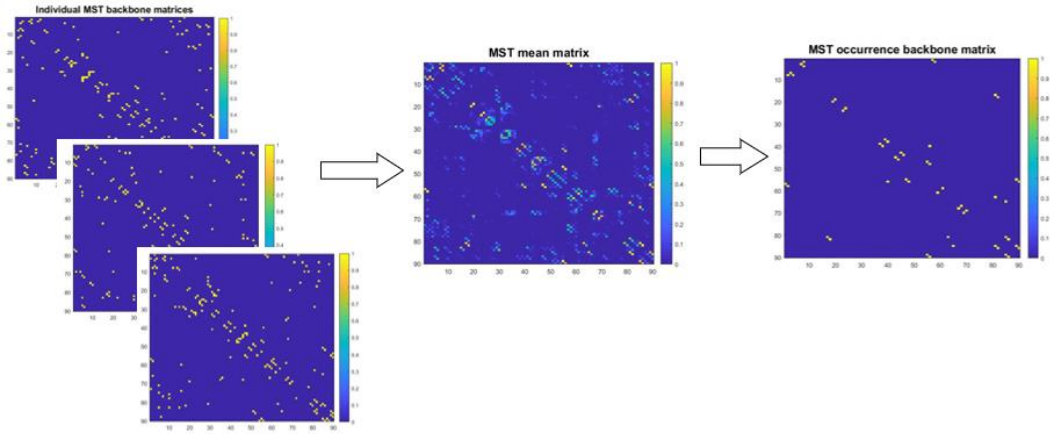

Figure 3.9 *- Pipeline for the reconstruction of the occurrence backbone matrix. Example with MST.*

On the other hand, the group average backbone is calculated by a different approach. Using the individual NOS connectivity matrices from all subjects, we compute the average matrix of all NOS matrices, to obtain a NOS group average matrix. Lastly, we apply the backbone algorithm to that group average matrix, a group average backbone. An example with MST is shown in Figure 3.10.

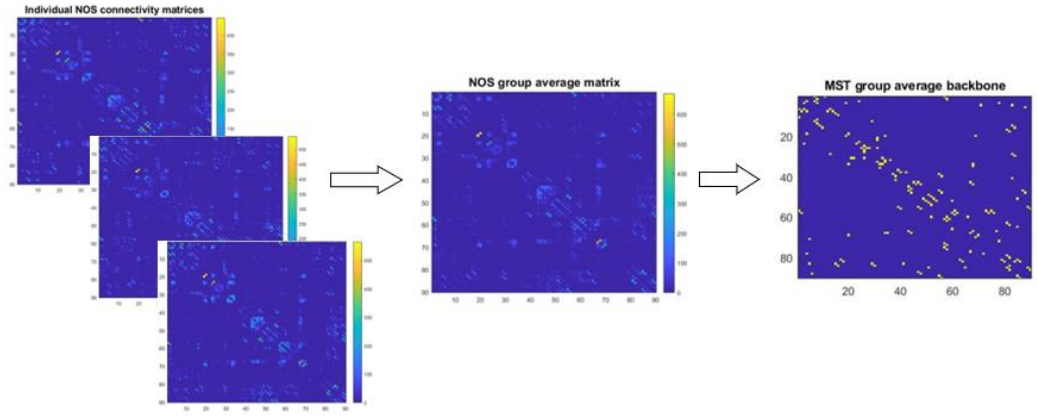

Figure 3.10 *- Pipeline for the reconstruction of the group average backbone matrix. Example with MST.*

3.2.3. MST measures

The MST has specific measures that can be calculated and used for further analysis. Therefore, to study the behavior of MST measures over two different time-points, we computed the following metrics that characterize MST: Diameter, Leaf Fraction, Degree Divergence and Tree Hierarchy[10,20,112]. A schematic image is shown in Figure 3.11.

The degree is the number of edges connected to a node. Therefore, the degree is a measure of regional importance, and as mentioned before, nodes with a high degree may be considered Hubs i.e., crucial regions on the functional brain network. Consequently, Degree Divergence is a measure of broadness of the degree distribution.

The Diameter is considered the longest shortest path of the MST, characterizing the largest distance between any two nodes, normalized for the total number of connections, $D = d/M$, where M is the total number of connections. It measures the efficiency of global network organization. In a network with a low diameter, information is efficiently processed between remote brain regions.

Leaf Fraction is the fraction of nodes that have only one connection (degree = 1), also called Leaf number (L), divided by the maximum possible number of connections (M): $L_t = L/M$. When the Leaf number is high, communication is essentially dependent on hub nodes.

Tree Hierarchy characterizes a hypothesized optimal topology of efficient organization while preventing information overload of central nodes. For a line-like topology Th = 0, for a star-like topology Th = 0.5, and for trees with a configuration between these 2 extreme situations, tree hierarchy can have values of Th ≈ 1.

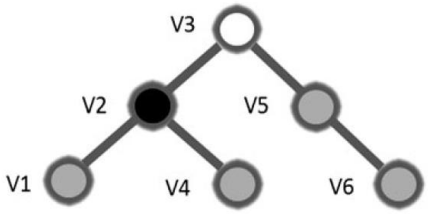

Figure 3.11 *- Example of a simple minimum spanning tree (MST) and its characteristics. V1, v4 and v6 are Leaf nodes, as they have a degree of 1. The diameter is the longest distance between any two nodes. In this tree, node v1 and v6 are most distant and the diameter has value of 4. Node v2 has the highest degree since it is connected to three other nodes. Image adapted from the paper of Boerma M.*[112]

In the case of MST measures, as the values between those measures are very distinct, we transformed every value *x* in a z-score value[125], that is calculated using:

$$Z = \frac{x-\mu}{\sigma} \tag{3.2}$$

where μ is the mean of the data set and σ its standard deviation. An absolute value of z represents the distance between that raw score *x* and the data set mean in units of the standard deviation. z is negative when the raw score is below the mean, positive when above. In our study, when comparing baseline vs

follow-up or controls vs patients, the Z-scores were always based on the mean and SD of baseline/controls values, to test the relative differences from that initial group.

3.2.4. Detection of SVD-related network impairments

The second question we addressed was whether our backbones can be sensitive to disease effects and if they are able to detect disease progression over time. For this approach we need to use graph metrics to perform backbone comparison between patients and controls.

In this study we therefore obtained measures of global connectivity (e.g. global efficiency) and local connectivity (e.g. node strength) from the FA- and MD-weighted networks. These weighted networks are frequently used to examine structural aspects of brain connectivity in patients and have been shown to be sensitive to the effects of SVD[41,43,126]. Global efficiency was defined as the inverse of the shortest path lengths (i.e. the minimum number of connections between each pair of brain regions), and expresses the extent to which information is exchanged over the network[90]. Connectivity strength was defined as the mean value of the FA- and MD- weighted matrices for each backbone network.

All graph measures mentioned in this manuscript were calculated using the brain connectivity toolbox[90] (https//sites.google.com/site/bcnet).

3.3. STATISTICAL ANALYSIS

Statistical analysis was performed using IBM SPSS statistics version 25 (IBM Corp. Released 2017. IBM SPSS Statistics for Windows, Version 25.0. Armonk, NY: IBM Corp). A p-value < 0.05 was considered significant.

For the binary MST measures analysis, we used two approaches: (1) paired-samples t-test for the within-subjects analysis, in Section 4.1.1 for the 90-nodes template and in Section 4.3.1., for the other two brain templates, and (2) independent-samples t-test for across-groups analysis, in Section 4.1.3.

For the cross-sectional analysis (Section 4.2.1), we analyzed between-group differences (SVD versus controls) in weighted graph metrics such as node strength (Section 4.2.1-a) and weighted global efficiency (Section 4.2.1.-b), using independent-samples t-test.

Finally, for the longitudinal analysis (Section 4.2.2.), we analyzed changes in patients' backbones weighted graph metrics (global efficiency and strength) over time, using ANOVA repeated measures, respectively in Sections 4.2.2-a and 4.2.2-b.

4. Results

4.1. Testing Reproducibility

This first part of the results concerns the 90-nodes template and is divided in three parts: (1) Reproducibility within subjects, where we compare scan-rescan backbones of controls and patients, separately, at different time-points; (2) Consistency across-subjects, where networks from baseline from each control subject are compared with an occurrence baseline network from all subjects; (3) Consistency across-groups, where we use two approaches: the first one is comparing the mean matrix with a minimum of 75% common edges between controls and patients at baseline; the second one is comparing the group average backbone matrix between controls and patients, also at baseline. As aforementioned, the comparison of the networks referred ahead was performed by calculating the mean between the dice overlap with the topology zeros overlap, giving a number between 0 and 1, that represents the edge-edge overlap.

4.1.1. Within-subject reproducibility

To compare the reproducibility of the backbones within-subjects, we overlapped the whole backbone networks of each subject from both time-points and used the values to build the plots from Figure 4.1. These boxplots show the network overlap between backbones reconstructed at baseline and follow-up for each subject, representing the reproducibility values on an individual level. Data of validation (left) and patients (right) were analyzed separately. The reproducibility mean and standard deviation (SD) values are shown in Table 4.1.

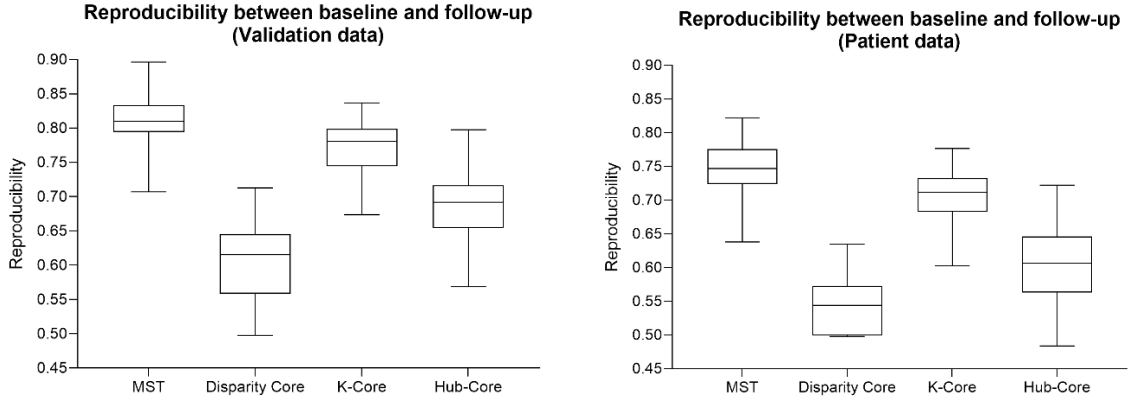

Figure 4.1 - *Backbone reproducibility of network backbones over two time-points: baseline and follow-up regarding validation data (left) and patient (right) data.*

Table 4.1 *- Network reproducibility (mean and SD) between baseline and follow-up.*

Backbone	Validation data	Patients
MST	0.805 ± 0.040	0.746 ± 0.037
Disparity Core	0.613 ± 0.068	0.544 ± 0.038
K-Core	0.772 ± 0.039	0.705 ± 0.043
Hub-Core	0.688 ± 0.069	0.602 ± 0.056

Regarding the MST backbone, we also examined how the characteristic binary MST metrics vary between time-points. The values of the MST measures on each time point are shown in Figure 4.2. Validation data is displayed on the left plot whereas data of SVD patients is shown on the right.

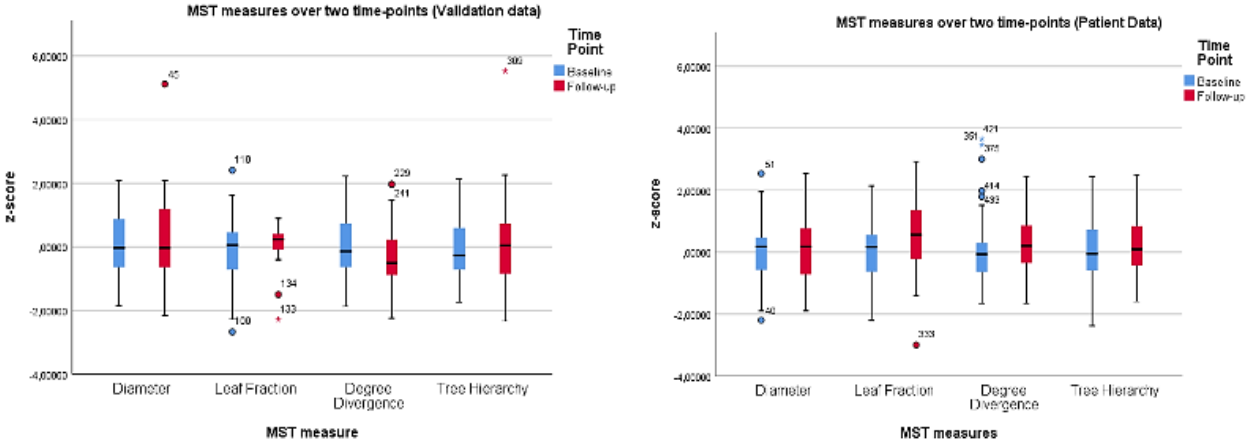

Figure 4.2 *- Binary MST measures comparison between baseline and follow-up for validation data (left) and patients (right). All z-scores are based on the mean and SD values at baseline.*

To analyze the relationship between MST measures over time in more detail we performed paired-sample t test for validation data and for patients. Regarding validation data reproducibility (Table 4.2), none of the MST measures differed statistically from baseline to follow-up, whereas considering patients (Table 4.3), Leaf Fraction was considered statically different between baseline (M = 0.468, SD = 0.029) and follow-up (M = 0.484, SD = 0.03), t (84) = -3.784, p < 0.001, and Degree Divergence was marginally significant (t (84) = -1.950 , p = 0.055).

Table 4.2 *- Results from paired sample t-test for validation data, using MST measures z-score values (mean ± SD) for time-points comparison.*

MST measures	Baseline (Mean ± SD)	Follow-up (Mean ± SD)	p-value
Diameter	0.271 ± 0.037	0.278 ± 0.049	0.360
Leaf Fraction	0.470 ± 0.029	0.464 ± 0.031	0.268
Degree Divergence	2.675 ± 0.091	2.649 ± 0.091	0.120
Tree Hierarchy	1.101E-05 ± 1.659E-06	1.112E-05 ± 2.13E-06	0.752

Table 4.3 *- Results from paired sample t-test for patients, using MST measures z-score values (mean ± SD) for time-points comparison.*

MST measures	Baseline	Follow-up	p-value
Diameter	0.263 ± 0.038	0.268 ± 0.035	0.343
Leaf Fraction	0.467 ± 0.028	0.484 ± 0.031	< **0.01**
Degree Divergence	2.682 ± 0.121	2.715 ± 0.101	0.042
Tree Hierarchy	1.08E-05 ± 1.591E-06	1.109E-05 ± 1.441E-06	0.185

4.1.2. Consistency across-subjects

To compare backbone consistency across subjects (within the Control group and the Validation data group), we calculated one occurrence backbone for each network backbone. Then, we overlapped the matrix of each subject with the occurrence matrix. For example, the MST matrix of each subject was compared with the MST occurrence backbone for that group. The results are shown in Figure 4.3.

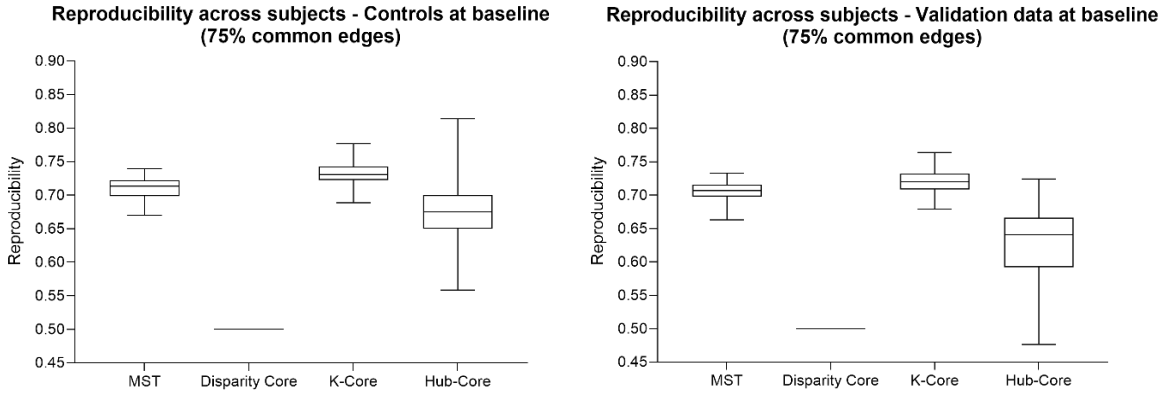

Figure 4.3 – *Reproducibility results of the comparison across-subjects for controls (left) and validation data (right) at baseline. Comparison with the occurrence matrix that has edges common in at least 75% of the subjects.*

Table 4.4 *- Reproducibility across-subjects regarding control and validation data group.*

Occurrence backbone (>75% edges correspondence)	Controls	Validation data
MST	0.712 ± 0.017	0.708 ± 0.017
Disparity Core	0.500 ± 0.000	0.500 ± 0.000
K-Core	0.731 ± 0.018	0.721 ± 0.018
Hub-Core	0.679 ± 0.048	0.627 ± 0.053

Besides the observation of the boxplots shown in Figure 4.3, the values displayed on Table 4.4 support that K-Core is the most consistent backbone across subjects at baseline for both groups. The Disparity

Core showed poor consistency across subjects because the 75% common-edges matrix had an insufficient number of connections, therefore, the correspondence values with the rest of the group backbone matrices are inconclusive.

4.1.3. Consistency across-groups

To analyze the consistency across groups (controls and patients), we compared the values at the same time-point: baseline. Therefore, we created one occurrence backbone matrix for each group, and we tested the similarity between these two matrices. Alternatively, group average backbones were also calculated for both groups. On both methods, we applied the network overlap, using only two backbone matrices: one from controls and the other from patients. For example, the MST occurrence backbone of the controls was compared with the MST occurrence backbone of the patients and the same was done with every group average backbone. That is why there is only one number in the values of Table 4.5.

Table 4.5 *- Similarity between patients and controls. Overlap between controls and patients at baseline.*

Backbone	"occurrence backbone" (>75% edges correspondence)	Group average backbone
MST	0.8332	0.8391
Disparity Core	0.000	0.5000
K-Core	0.8259	0.7573
Hub-Core	0.8211	0.7811

In order to study the behavior of MST measures across both groups, we performed MST metrics comparison at baseline between control and patient data. Figure 4.4 shows the z-scores of each measure for both groups. Table 4.6 shows the statistic parameters of independent samples t-test. As all the p-values are higher than 0.05, none of the MST metrics differ statistically between controls and patients at baseline.

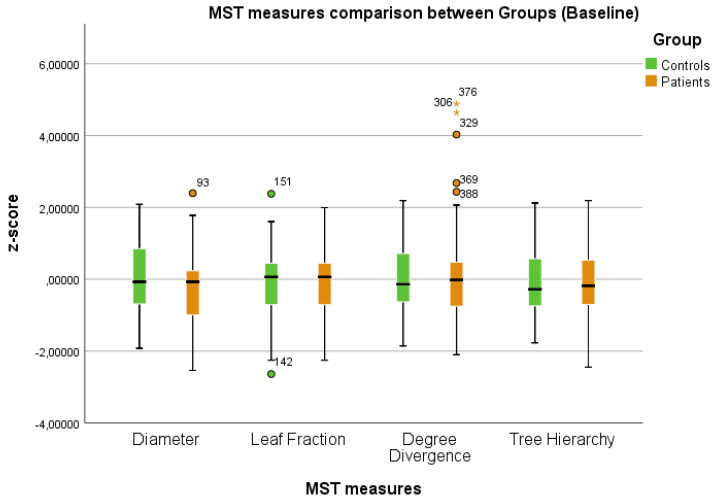

Figure 4.4 *- Binary MST measures z-score values across groups at baseline. All z-scores are based on the mean and SD of controls.*

Table 4.6 - *Results from independent samples t-test for baseline, using MST measures z-score values (mean ± SD) for group comparison*

MST measures	Controls	Patients	p-value
Diameter	0.272 ± 0.036	0.262 ± 0.038	0.173
Leaf Fraction	0.470 ± 0.029	0.464 ± 0.031	0.631
Degree Divergence	2.676 ± 0.092	2.68 ± 0.12	0.749
Tree Hierarchy	1.105E-05 ± 1.652E-06	1.08E-05 ± 1.57E-06	0.417

4.2. TESTING SENSITIVITY TO DISEASE EFFECTS AND PROGRESSION

4.2.1. Cross-sectional analysis

a) Node Strength

To test whether these backbones are sensitive to disease effects, we compared Fractional Anisotropy (FA), Mean Diffusivity (MD) weighted networks between controls and patients at baseline, using node strength. Figure 4.5 shows the z-score values of MST network weights and its comparison between groups. The information about the other backbones' network weights can be found on the results from the independent samples t-test in Table 4.7. The differences between controls and patients are all significantly different between baseline and follow-up ($p < 0.01$).

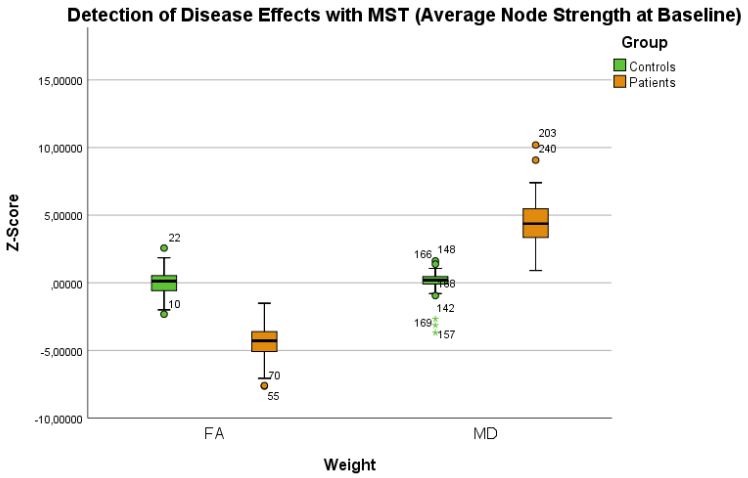

Figure 4.5 *- MST network weights (FA and MD using node strength) comparison between controls and patients at baseline. All Z-scores are based on the mean and SD of controls.*

Table 4.7 *- Results from independent samples t-test for baseline, using node strength (mean ± SD) backbone weights comparison.*

Network weights (Node Strength)	Controls	Patients	p-value
FA (MST)	0,307 ± 0,016	0,236 ± 0,021	**<0.01**
MD (MST)	0,826E-3 ± 4,34E-05	1,021E-3 ± 7,232E-05	**<0.01**
FA (Disparity Core)	0,345 ± 0,034	0,280 ± 0,042	**<0.01**
MD (Disparity Core)	0,833E-3 ± 5,29E-05	1,001E-3 ± 0,0001	**<0.01**
FA (K-Core)	0,342 ±0,013	0,278 ± 0,019	**<0.01**
MD (K-Core)	0,856E-3 ± 5,29E-05	1,034E-3 ± 7,190E-05	**<0.01**
FA (Hub-Core)	0,359 ± 0,016	0,292 ± 0,021	**<0.01**
MD (Hub-Core)	0,835E-3 ± 4,83E-05	0,994E-3 ± 7,420E-05	**<0.01**

b) Weighted Global Efficiency

The same approach was applied but this time based on global efficiency. Figure 4.6 shows the comparison between groups, using z-score values of MST network weights. The independent samples t-test results for MST and the other backbones are shown in Table 4.8. patients had a lower GE than controls in every backbone ($p < 0.01$), except the MD-weighted GE in K-Core ($p = 0.012$).

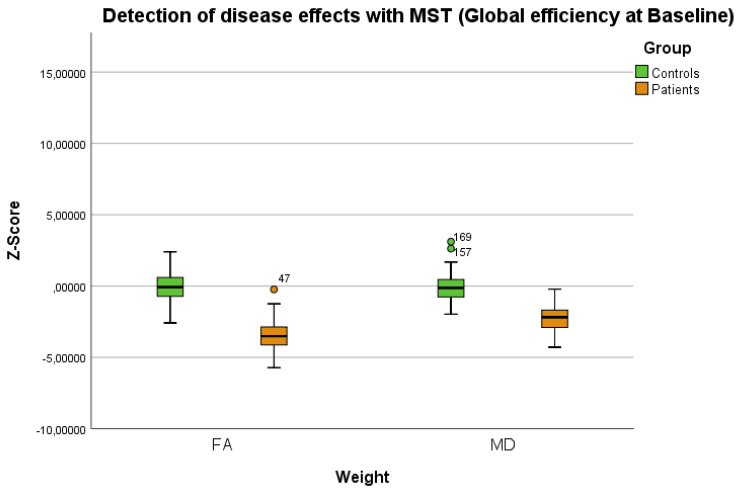

***Figure 4.6** – Comparison of global efficiency z-scores of MST network weights (FA and MD) between controls and patients at baseline.*

***Table 4.8** - Results from independent samples t-test for baseline, using global efficiency (mean ± SD) backbone weights comparison.*

Network weights (Global efficiency)	Controls	Patients	p-value
FA (MST)	0,048 ± 0,004	0,035 ± 0,004	**<0.01**
MD (MST)	195,084 ± 14,863	161,190 ± 13,609	**<0.01**
FA (Disparity Core)	0,002 ± 0,002	0,001 ± 0,001	**<0.01**
MD (Disparity Core)	8,229 ± 4,810	4,927 ± 2,963	**<0.01**
FA (K-Core)	0,106 ± 0,020	0,093 ± 0,018	**<0.01**
MD (K-Core)	345,688 ± 69,302	314,308 ± 57,824	**0.012**
FA (Hub Core)	0,201 ± 0,011	0,155 ± 0,016	**<0.01**
MD (Hub Core)	653,306 ± 43,557	540,852 ± 49,428	**<0.01**

4.2.2. Longitudinal analysis

In this part of the project, we tested the differences between baseline and follow-up for patients in order to understand which backbone is more sensitive to disease progression. Statistical analysis was done with repeated measures in SPSS.

a) Changes in Node Strength

Changes in node strength regarding FA and MD are shown on figures 4.7 and 4.8, respectively. We used Repeated measures ANOVA to test the disease progression. Tables 4.9 and 4.10 summarize the results regarding FA-weighted and MD-weighted networks for each backbone. The node strength of all backbones decreased significantly between baseline and follow-up (p-value < 0.05).

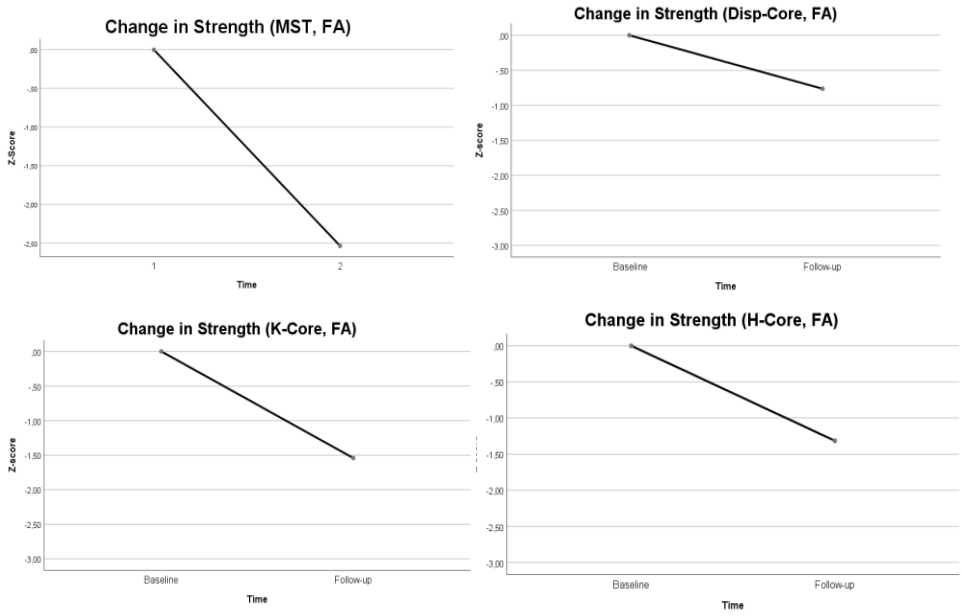

Figure 4.7 - *Changes in node strength regarding FA, analyzed on the backbone networks of patients between baseline and follow-up.*

Table 4.9 -*Repeated measures ANOVA regarding FA-weighted network node strength changes.*

Network backbone	Effect	df_1	df_2	F	p-value
MST	Time	1	86	671.415	< **.001**
Disparity Core	Time	1	86	33.888	< **.001**
K-Core	Time	1	86	69.962	< **.001**
Hub Core	Time	1	86	174.464	< **.001**

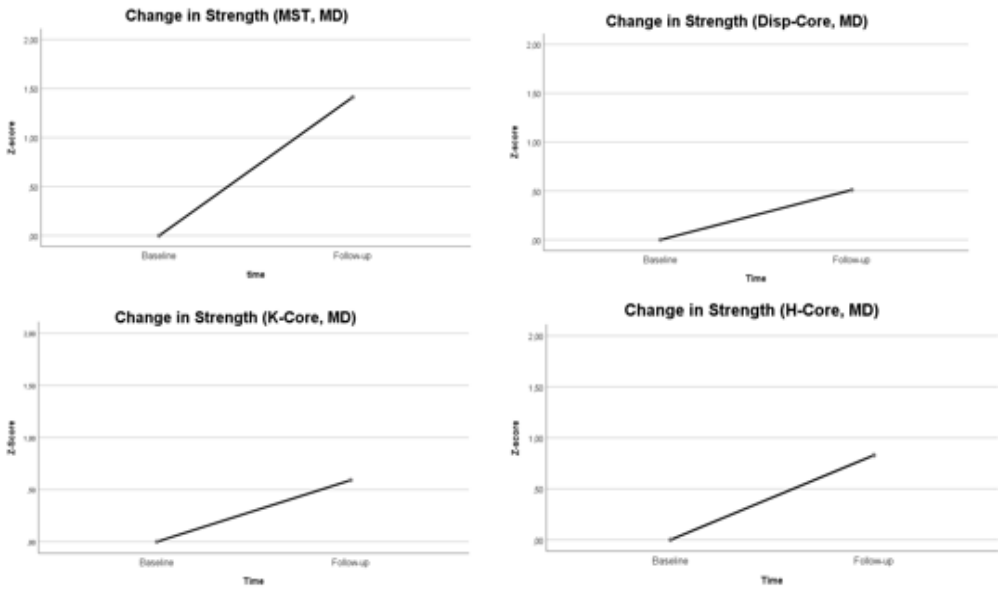

Figure 4.8 *- Changes in node strength regarding MD, analyzed on the backbone networks of patients between baseline and follow-up.*

Table 4.10 *- Repeated measures ANOVA regarding MD-weighted network node strength changes.*

Network backbone	Effect	df_1	df_2	F	p-value
MST	Time	1	86	231.008	< **.001**
Disparity Core	Time	1	86	12.245	< **.001**
K-Core	Time	1	86	5.303	**0.024**
Hub Core	Time	1	86	64.481	< **.001**

b) Changes in Global Efficiency

Changes in global efficiency regarding Fractional Anisotropy and Mean Diffusivity are shown on figure 4.9 and 4.10, respectively. We also used Repeated measures ANOVA to test the disease progression. The results regarding FA-weighted and MD-weighted networks for each backbone are summarized on table 4.11 and 4.12, respectively. The global efficiency of all backbones decreased significantly between baseline and follow-up (p-value < 0.05), except for the Hub-Core that increased.

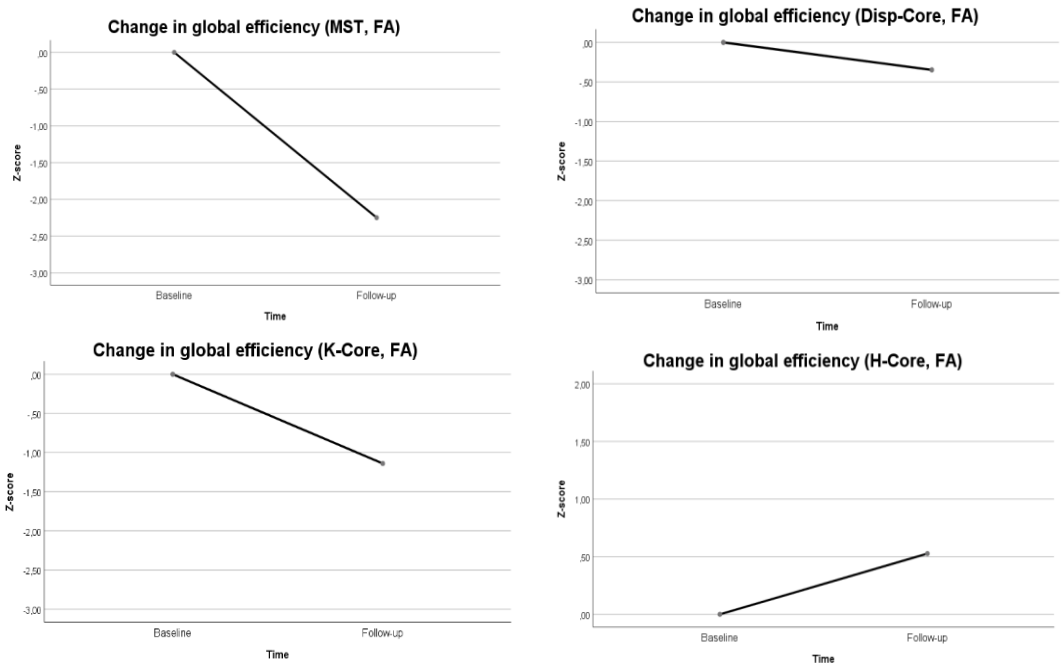

Figure 4.9 *- Changes in global efficiency regarding FA-weighted networks, analyzed on the backbone networks of patients between baseline and follow-up.*

Table 4.11 - Repeated measures ANOVA regarding FA-weighted network global efficiency changes.

Network backbone	Effect	df_1	df_2	F	p-value
MST	Time	1	86	396.274	< **.001**
Disparity Core	Time	1	86	9.749	**<.01**
K-Core	Time	1	86	41.784	< **.001**
Hub-Core	Time	1	86	27.425	< **.001**

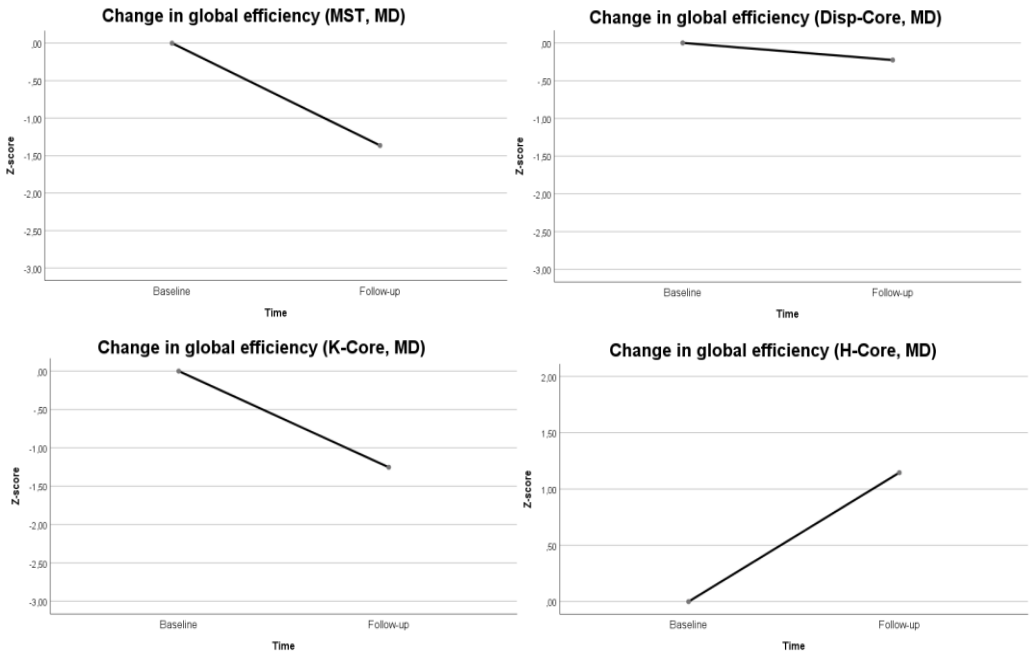

Figure 4.10 *- Changes in global efficiency regarding MD-weighted networks, analyzed on the backbone networks of patients between baseline and follow-up.*

Table 4.12 *- Repeated measures ANOVA regarding MD-weighted network global efficiency changes.*

Network backbone	Effect	df_1	df_2	F	p-value
MST	Time	1	86	118.160	< **.001**
Disparity Core	Time	1	86	2.329	< **.001**
K-Core	Time	1	86	28.257	< **.001**
Hub-Core	Time	1	86	107.508	< **.001**

4.3. COMPARING DIFFERENT BRAIN LABELS (90, 200 AND 250 NODES)

In this part of the project, we compared the 90-nodes with the 200-nodes whole-brain backbones as well as with the 250-nodes backbones for the left hemisphere. Due to time constrains in image processing, we only computed the 200 and 250-node networks (from baseline and follow-up) for the validation dataset. Thus, our analysis regarding these networks was restricted to within- and across-subjects comparisons, and not across groups. Therefore, we performed three tests: the reproducibility within-subjects, that is, the comparison between time-points for each backbone; the MST measures reproducibility between time-points and, finally, the consistency across-subjects, at baseline.

4.3.1. Within-subjects reproducibility

As previously done with the 90-nodes only, we also performed a comparison of the reproducibility within-subjects with the 200 whole-brain and 250 left hemisphere nodes templates. Accordingly, we overlapped the networks of each subject from both time-points and used the reproducibility values to build the plots shown in Figure 4.11 and 4.12. The dataset from validation data group with 90 nodes (left) and 200 nodes (right) were analyzed separately.

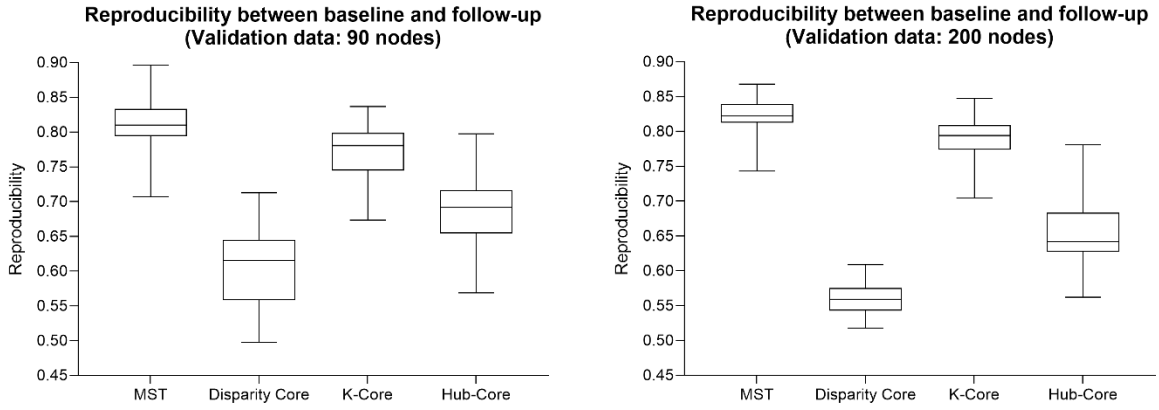

Figure 4.11 - *Backbone reproducibility of network backbones over two time-points: baseline and follow-up regarding validation data 90-nodes (left) and 200-nodes (right) data.*

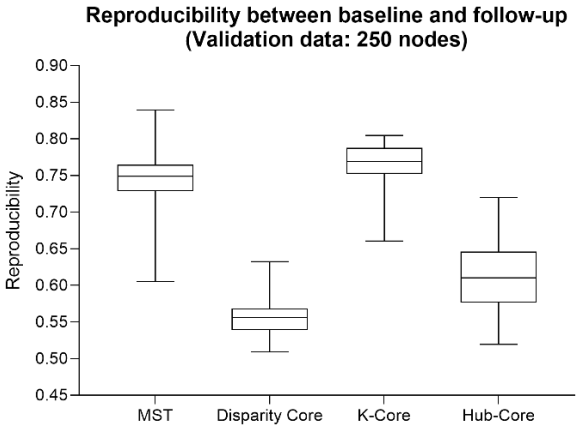

Figure 4.12 *- Backbone reproducibility of left-hemisphere network backbones between baseline and follow-up regarding 250-nodes (right) data.*

To analyze the data from this comparison, we used edge-edge overlap and group average backbone approaches. The results shown on Table 4.13 are based on Figures 4.11 and 4.12 and represent the reproducibility values on an individual level. On the other hand, Table 4.14 presents the values of the similarity between these group average backbones (baseline average backbone vs follow-up average backbone).

Table 4.13 *- Network reproducibility (mean ± SD) between baseline and follow-up.*

Backbone	**90-nodes template (whole-brain)**	**200-nodes template (whole-brain)**	**250-nodes template (left-hemisphere only)**
MST	0.805 ± 0.040	0.813 ± 0.045	0.742 ± 0.046
Disparity Core	0.613 ± 0.068	0.559 ± 0.023	0.556 ± 0.026
K-Core	0.772 ± 0.039	0.787 ± 0.035	0.764 ± 0.034
Hub-Core	0.688 ± 0.069	0.651 ± 0.043	0.610 ± 0.048

Table 4.14 *- Group average backbone similarity between baseline and follow-up.*

Average backbone reproducibility	**90-nodes template (whole-brain)**	**200-nodes template (whole-brain)**	**250-nodes template (left-hemisphere only)**
MST	0.948	0.959	0.915
Disparity Core	0.750	0.549	0.556
K-Core	0.909	0.645	0.907
Hub-Core	0.508	0.582	0.626

Interestingly, on average the group-level backbone is very reproducible between time points. Besides that, the K-Core is the best backbone regarding one-hemisphere reproducibility over time, whilst whole-brain reproducibility has the MST as the better one either by using the 90 nodes as well as the 200 nodes labels.

Regarding MST metrics, the results of the reproducibility from each time point are shown in Figure 4.13 comparing the consistency over time regarding the 90-nodes (left) and the 200-nodes (right) backbones from the validation data. The results using 250-nodes template of the left hemisphere is shown in Figure 4.14.

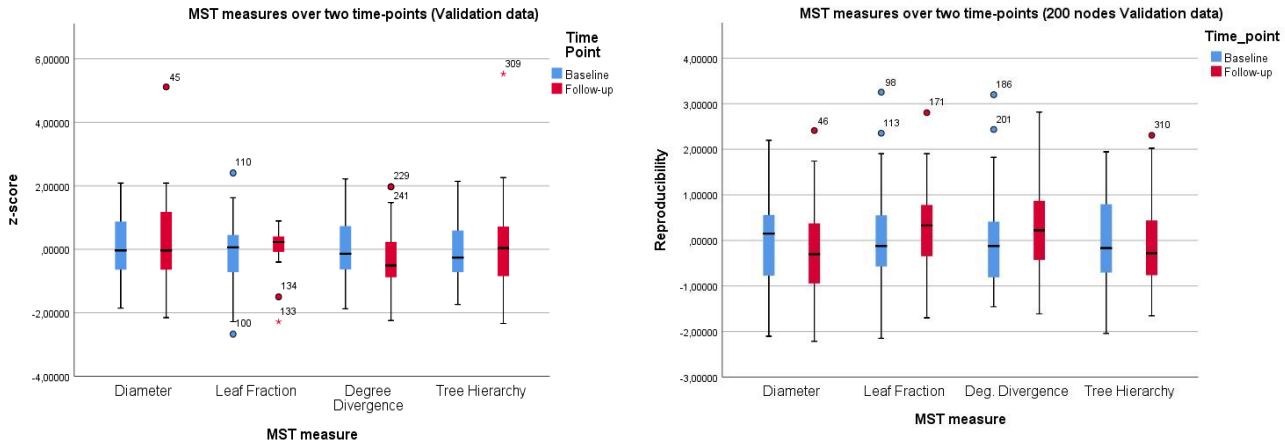

***Figure 4.13** – Binary MST measures comparison between baseline and follow-up for 90-nodes (left) and 200-nodes (right) templates for validation data. All z-scores are based on the mean and SD values at baseline.*

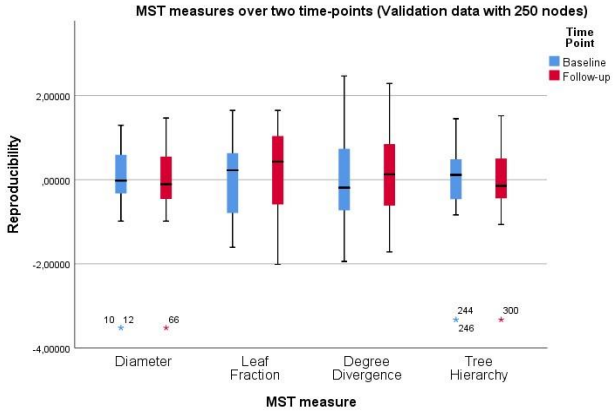

***Figure 4.14** – Binary MST measures comparison between baseline and follow-up for the 250-nodes left hemisphere network. Z-scores are based on the mean and SD values at baseline.*

Similar to the 90-nodes template where we compared the validation data group with the patients group, here we analyzed the relationship between MST measures over time regarding the other two templates, and compared the results with the ones obtained previously with the 90-nodes. In order to perform this comparison, we performed paired sample t-test for each group. The results of the tests are shown in Tables 4.15 to 4.17, where it is clear that the MST measures don't differ significantly between time-

points regarding a stable group like this validation data group, which means that these are consistent measures for both 90 and 200-nodes template, as well as for the 250-nodes from the left hemisphere.

Table 4.15 - *Results from paired sample t-test applied to the MST measures z-score values (mean ± SD) of the 90-nodes validation data, for time-points comparison.*

MST measures	Baseline	Follow-up	p-value
Diameter	0.271 ± 0.037	0.278 ± 0.049	0.360
Leaf Fraction	0.470 ± 0.029	0.464 ± 0.031	0.268
Degree Divergence	2.675 ± 0.091	2.649 ± 0.091	0.120
Tree Hierarchy	1.101E-05 ± 1.659E-06	1.112E-05 ± 2.13E-06	0.752

Table 4.16 - *Results from paired sample t-test applied to the MST measures z-score values (mean ± SD) of the 200-nodes validation data, for time-points comparison.*

MST measures	Baseline	Follow-up	p-value
Diameter	0.441 ± 0.055	0.437 ± 0.053	0.236
Leaf Fraction	0.405 ± 0.022	0.410 ± 0.022	0.191
Degree Divergence	2.578 ± 0.066	2.596 ± 0.069	0.204
Tree Hierarchy	1.604E-07 ± 2.223E-07	1.578E-07 ± 1.980E-07	0.533

Table 4.17 - *Results from paired sample t-test applied to the MST measures z-score values (mean ± SD) of the 250-nodes left hemisphere of validation data group, for time-points comparison.*

MST measures	Baseline	Follow-up	p-value
Diameter	0.452 ± 0.128	0.447 ± 0.108	0.838
Leaf Fraction	0.465 ± 0.019	0.469 ± 0.022	0.359
Degree Divergence	2.804 ± 0.089	2.813 ± 0.088	0.613
Tree Hierarchy	8.561E-07 ± 2.572E-07	8.334E-07 ± 2.109E-07	0.651

5.3.2. Consistency across-subjects

To compare backbone consistency across subjects, we calculated the occurrence backbone for each backbone of the validation data group at baseline. Then, using this matrix as a comparison term to test the reproducibility across subjects, we overlap the matrix of each subject with this occurrence matrix, as we did before just for the 90-nodes template. The results for this analysis are shown in Figure 4.15 and 4.16, and in Table 4.18.

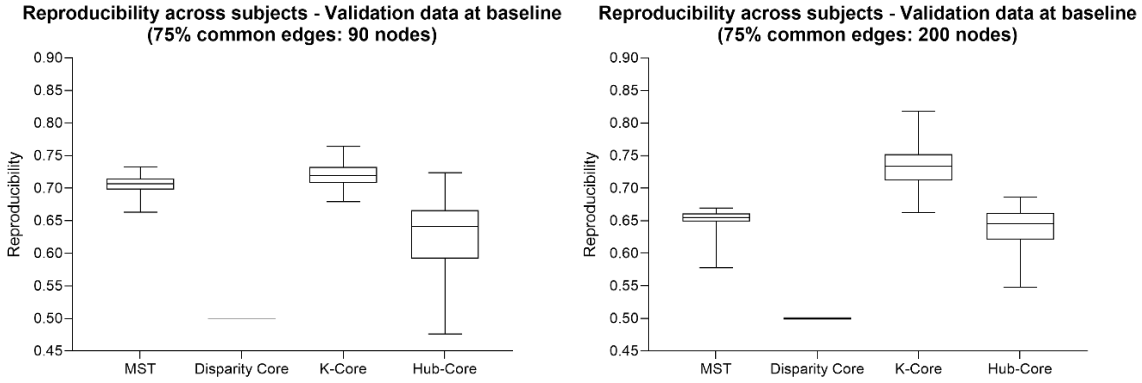

Figure 4.15 - *Reproducibility for the consistency of backbones at baseline. Validation data with 90-nodes template (left) and 200-nodes template (right). Comparison with the occurrence matrix that has edges common in at least 75% of the subjects.*

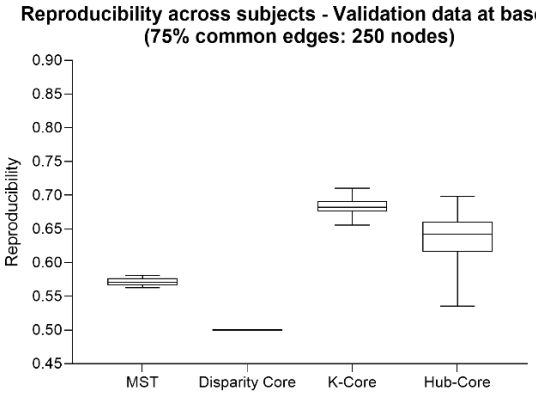

Figure 4.16 - *Reproducibility for the consistency of backbones at baseline. Validation data using the 250-nodes left hemisphere template. Comparison with the occurrence matrix that has edges common in at least 75% of the subjects.*

Table 4.18 - *Consistency given by reproducibility (mean ± SD) across subjects on control group and validation data group.*

"occurrence backbone" (>75% edges correspondence)	**90-nodes backbone**	**200-nodes backbone**	**250-nodes left-hemisphere backbone**
MST	0.708 ± 0.017	0.651 ± 0.016	0.571 ± 0.007
Disparity Core	0.500 ± 0.000	0.500 ± 0.000	0.500 ± 0.000
K-Core	0.721 ± 0.018	0.736 ± 0.027	0.681 ± 0.015
Hub-Core	0.627 ± 0.053	0.637 ± 0.031	0.629 ± 0.046

5. Discussion

In this study, we investigated whether network backbones can be used in clinical datasets as a structural architecture of the human brain network, by testing if they are reproducible over time and sensitive to disease effects and disease progression in patients with SVD. Our results suggest that network backbones can be used in clinical approaches due to their reproducibility and sensitivity to disease effects. MST is the backbone that presents the best results and therefore the best one to be used in these cases.

5.1. Reproducibility within- and across- subjects and consistency across groups

In the first part of our analysis (Section 4.1.), we started by testing the reproducibility and consistency of the 90-nodes network backbones, performing within-subjects, across-subjects and across-groups analysis. Regarding within-subject reproducibility (Section 4.1.1.), we first analyzed the whole-network backbone reproducibility and then the differences between baseline and follow-up of the MST measures. Analyzing the values of network reproducibility between baseline and follow-up presented in Figure 4.1 and Table 4.1, it is easily noticed that the best overall reproducibility values are achieved by validation data compared to the group of patients. We can hypothesize that the healthy subjects have more similarity between them concerning the most important and structural connections of the brain than the group of patients diagnosed with SVD. This can be explained by the differences of connectivity alterations, expected by different SVD markers within the group. Furthermore, the best reproducibility values are achieved using MST, with 0.805 ± 0.040 and 0.746 ± 0.037, for both validation and patient data respectively, whereas Disparity Core has apparent limitations compared to the rest of the backbones, with a reproducibility of 0.613 ± 0.068 and 0.544 ± 0.038 for each group respectively. Accordingly, MST seems to be the backbone that better represents the structural connections that are common between time-points within the same subject. Regarding MST backbone measures values, displayed in Figure 4.2, it is possible to conclude that they are consistent within subjects, as they do not change statistically between time-points. However, although none of the MST measures in validation data suffer significant changes over time (Table 4.2), Leaf Fraction shows a significant difference between baseline and follow-up in patients (Table 4.3), from which we can infer that, in patients with SVD, the number of nodes with a degree of one can increase over time, as connections are becoming weaker due to disease.

Studying the reproducibility across-subjects of the four backbones at baseline (Section 4.1.2.), over the set of controls and validation data groups, it is possible to conclude that K-Core is the most consistent backbone, by looking at Figure 4.3 and Table 4.4. K-Core presents a reproducibility of 0.731 ± 0.018 and 0.721 ± 0.018, followed by MST with 0.712 ± 0.017 and 0.708 ± 0.017, for controls and validation data groups respectively. K-Core and MST have a good stability when comparing the backbone of each subject with the backbone that has only connections present in 75% of the subjects. The Disparity Core has poor results: the network overlap given by the reproducibility between each subject and the occurrence backbone is 0.500 ± 0.000, as the dice overlap is null (0) and the topology zeros overlap, or the overlap of zeros between two matrices, is total (1). This happens because the 75% common-edges occurrence matrix for Disparity Core had no edges at all, therefore the values of correspondence between the occurrence backbone and each subject's backbone are meaningless.

In order to compare the consistency across groups (Section 4.1.3.), firstly we performed network analysis between controls and patients at baseline using occurrence backbone and group average backbone, and

then we studied MST measures changes between controls and patients at baseline. Thus, we started by creating four occurrence backbone matrices (with more than 75% common edges) for controls and patients and tested the similarity between each of these four pairs of matrices, at baseline. Similarly, we compared the four pairs of group average backbones between controls and patients, also at baseline. The values of reproducibility are shown in Table 4.5. We conclude that, except Disparity Core (it has insufficient number of nodes in its occurrence matrix), all backbones have a good consistency across groups. Moreover, the differences shown in Table 4.5 indicate that K-Core is the one that shows the less similarity between group average backbones of controls and patients; therefore, it can be a useful backbone to distinguish these two groups. Furthermore, as the overall occurrence backbone similarity values of all backbones are higher than the group average backbone values, we can conclude that the nodes and connections that are present in at least 75% of the subjects are more representative of the common network structure between healthy subjects and SVD-patients. This is important to highlight because the weaker connections might disappear due to disease, explaining the lower similarity between the average connections of these groups. Regarding the MST measures between controls and patients presented in Figure 4.4, they show virtually no significant differences. In Table 4.6 it is visible that these values do not differ statistically, and again we conclude that MST metrics are consistent across controls and patients. Therefore, it is not advantageous to use MST metrics to see differences between these groups.

5.2. Testing sensitivity to disease effects and disease progression

For the second part of our analysis (Section 4.2.), we studied the detection of disease effects in a cross-sectional way, by analyzing networks of patients and controls at baseline; and lastly we studied the detection of disease progression, in a longitudinal analysis, to compare the backbone network changes on patients over time, between baseline and follow-up.

In the cross-sectional analysis (Section 4.2.1.), the changes between controls and patients using FA and MD matrices are visible in Figures 4.5 and 4.6, regarding both node strength and weighted global efficiency, respectively. Every backbone has significant differences between controls and patients (Tables 4.7 and 4.8). Additionally, every backbone showed practically the same behavior about these network weights: regarding average node strength, as expected, FA decreases from baseline to follow-up, while MD increases. This is expected from the literature, because decreases in FA and increases in MD values are indicative of loss of tissue integrity, supporting the concept that white matter microstructural changes are likely to contribute to the decline in cognitive function[8,9,63]. With respect to global efficiency values of FA and MD-weighted matrices, the results show that they are always lower at follow-up. This supports the hypothesis that SVD condition diminishes global efficiency in the brain network, as the neuronal pathways lose structure and white matter becomes disrupted. Moreover, we verify that the values of global efficiency for the Hub Core are very high compared to the other backbones. We hypothesize that this happens because it is composed by hubs, that are nodes with higher centrality and importance, evidencing that hubs can increase the efficacy of the communications on the network[16,114]. Finally, from these results it is clear that FA and MD node strength and global efficiency are good predictors of disease effects. These alterations of FA and MD values due to vascular dementia, had already been proved by literature, but have never been tested in network backbones.

In the longitudinal analysis (Section 4.2.2.), we wanted to test if the changes in node strength and global efficiency on patients regarding FA and MD, were significantly different between baseline and follow-

up. The goal was to test if the network backbones can detect disease progression in a reliable way. Figures 4.7 and 4.8 show the changes of node strength regarding FA and MD-weighted matrices, respectively. Tables 4.9 and 4.10 confirm that its values are significantly different between baseline and follow-up, for patients. These evidences show that it is possible detect disease progression by analyzing the node strength alterations in FA and MD-weighted matrices of backbone networks over time. Once again, as expected, FA values decreased and MD values increased between baseline and follow-up, due to the anomalies in the organization of the white matter tracts. Furthermore, concerning global efficiency, Figures 4.9 and 4.10 show the FA- and MD- weighted networks changes over time. Tables 4.11 and 4.12 present the values of these changes, where it is clear that global efficiency decreases significatively over time, due to disease development, except for Hub-Core, where global efficiency increases between baseline and follow-up. That might be due to the dependence of global efficiency on network density or number of connections, while node strength is independent of these conditions. This dependency on network density might cause some ambiguous results, illustrated, in this case, by the increased global efficiency in Hub-Core of patients over time, making global efficiency a less reliable predictor of disease-related network changes than node strength.

5.3. Comparing different brain labels

In the last part of our analysis (Section 4.3.), we used different brain parcellation schemes, of 200 and 250 nodes, to test if they would influence our results. Thus, using these two templates only for validation data (due to time constrains), we were able to perform within-subjects analysis, MST measures changes between time-points and consistency across-subjects, at baseline. Firstly, considering the whole-brain template of 200 nodes presented in Figure 4.11, it is visible that the reproducibility results within-subjects are consistent with the 90 nodes template, supporting that MST is the most reproducible backbone between time-points, with reproducibility values of 0.805 ± 0.040 and 0.813 ± 0.045 for 90 and 200 nodes templates respectively (Table 4.13). Disparity Core continues to present the lowest values of reproducibility: 0.613 ± 0.068 and 0.559 ± 0.023 for both templates, respectively. We can then conclude that MST is the most reproducible whole-brain backbone in terms of structure, and the most appropriate for this kind of analysis. However, regarding only the left hemisphere using the 250-nodes template (Figure 4.12), the K-Core shows the best reproducibility between time-points, with 0.764 ± 0.034, surpassing MST values of 0.742 ± 0.046. These results lead to the hypothesis that the connectivity concerning the left hemisphere is supported on sub-graphs of connectivity with more importance (higher degree). Furthermore, the group average similarity between baseline and follow-up (Table 4.14) shows very good results for MST concerning every template, with 0.948, 0.959 and 0.915 for 90, 200 and 250 nodes respectively; and K-Core regarding 90-nodes and 250-nodes, with values of 0.909 and 0.907 respectively. Once again, the MST backbone is the best backbone regarding reproducibility over time, followed by K-Core. Concerning the MST measures changes over time (Figures 4.13 and 4.14), as previously seen regarding the 90-nodes template, they all remain constant, regarding both the whole-brain templates and the left hemisphere 250-nodes template. Tables 4.15 to 4.17 shows that they do not change statistically between time-points. This supports once again the hypothesis that MST is a good backbone for reproducibility over time-points, as it maintains the stability of the network over time, and is not so influenced by noise and other artifacts or external factors caused by the inaccuracy of the diffusion MRI technique. Finally, the consistency across-subjects is tested comparing every network with the occurrence backbone for validation data at baseline for all three templates, shown in Figures 4.15 and 4.16. The values of correspondence between every subject and the occurrence backbone are

shown in Table 4.18, revealing that K-Core remains the best one regarding the connections that are present in 75% of the subjects, followed by MST with 90 and 200 nodes template, whereas Hub-Core has the second better reproducibility values regarding the 250 left hemisphere nodes template. Once again, we can hypothesize that brain connectivity concerning the left hemisphere is supported on sub-graphs of connectivity with more importance (higher degree). For all three templates, the Disparity Core keeps on having inconclusive results.

5.4. Final Remarks

Overall, our results answer the questions asked in the introduction of this study: we show that network backbones can be used in clinical approaches, as they are reproducible over time, and able to detect disease effects and progression. In terms of consistency and reproducibility over time within the same group of subjects, we demonstrated that MST and K-Core have the best results as they represent the structural connections and the connectivity core of the brain network.

Besides, we strengthen the notion that DTI parameters are advantageous in the study of the changes in the connectivity of the brain. FA and MD components of these backbones and their alterations through time, are directly in line with previous findings concerning changes in neuronal pathways due to disease development. The white matter disorganization is translated to the network backbone as a decreased anisotropy and increased mean diffusivity, due to the loss of structured diffusion. This supports the idea that network analysis can be very useful to study the evolution of SVD effects. Remarkably, we were able to detect disease progression using only a backbone of brain connections, that is not only sensitive to disease effects and progression, but also consistent within- and across-subjects. We therefore propose the use of MST as a reference network or standard backbone of the human connectome. As it is consistent within- and across- validation data subjects, it indicates that the majority of MST connections are similar in healthy adults, but individual connections may vary between subjects.

Together, the present findings confirm that the Minimum Spanning Tree is the best backbone regarding reproducibility between time-points and detection of disease effects, whereas node strength is the best approach to detect disease effects on the network backbone.

6. Conclusions

Modern network analysis is a rapidly growing field in neuroscience, but the lack of a proper methodology for network comparison between studies, and between conditions within studies, is increasingly becoming an important obstacle to further progress. In this study, we investigated whether network backbones can be used in clinical datasets as a structural architecture of the human brain network, by testing if they are reproducible over time and sensitive to disease effects and disease progression in patients with SVD.

Our results suggest that there are brain network backbones that can be applied to clinical datasets as they can detect disease changes and disease progression, while are also a reliable way to compare brain connectivity between time-points. Minimum Spanning Tree is the best backbone overall. It concedes a unique and consistent representation of a weighted network, while offering an adequate model to be used in a clinical situation, as it is reproducible either within and across-subjects, and the more stable backbone across groups at baseline. This goes along with some studies showing that MST provides an elegant and straightforward approach to analyze structural brain networks[10,20]. Besides, the strengths of using MST for brain network analysis rely in its properties: it is a mathematically defined, unbiased sub-network that reflects the most fundamental network properties, allowing for an unbiased comparison between networks of equal size in empirical studies. Moreover, in this study, it is demonstrated the efficacy of K-Core and MST to detect disease effects between controls and patients, as well as disease progression in patients between baseline and follow-up. However, at the same time, the uniqueness of the MST is also an advantage over K-Core, as the construction of the MST is independent of arbitrary thresholds or link weight transformations. Therefore, the present findings can help researchers to make a well-informed choice when selecting an appropriate network backbone for future clinical dataset studies.

The use of graph-theoretical network approaches is a relatively young scientific field in the context of neuroscience research. Although promising, this approach can be related with some methodological problems. Apart from the thresholding problem, there are other limitations associated with practical issues. First of all, the parcellation of the brain regions might influence the network properties. We used the AAL atlas that consists of unequal-sized 90 brain regions to parcel the brain for network construction. Thus, in order to achieve more comprehensive results, we also used two more templates. However, defining these brain regions remains challenging, and the extent to which different parcellation strategies might improve the results remains, however, unclear[127].

Moreover, our results corroborate studies showing that the vascular damage (indicated by conventional MRI markers for SVD) might be related to neurological dysfunction via reduced structural network efficiency[43,126]: the majority networks of our patients had lower global efficiency over time and lower node strength. Moreover, our results show that node strength was the strongest predictor for the loss of integrity over time. This analysis of disease progression over time is crucial, because besides the effects of focal damage by SVD on a single region, the cumulative effects of the SVD-related lesions distributed over the brain may also affect the integration of information communication (or the efficiency) between brain regions[41], which might lead to cognitive impairment over time. Therefore, these results highlight the relation between network efficiency and cognitive performance in participants with SVD, indicating

a significant role for network analysis in SVD-related cognitive deficits, in addition to conventional MRI markers.

Nonetheless, this study opens several innovative investigation possibilities. Firstly, it allows the study of brain connectivity not only locally but also globally by characterizing the topological features of this large-scale network. Mainly, we can use the individual tract properties or network statistics to globally characterize brain connectivity in an individual living subject. Such global characterizations are fundamental for a better understanding of brain communication. Second, our approach is non-invasive, efficient, individual and of relatively high-resolution. Our study may then contribute to the discovery of the general principles regulating communication, evolution, and development of the brain in a more reliable way; in clinical neuroscience it may shed new light into diseases of disorders that include disruptions of anatomical brain connectivity.

7. References

1. Knight MJ, McCann B, Kauppinen RA, Coulthard EJ. Magnetic resonance imaging to detect early molecular and cellular changes in Alzheimer's disease. *Front Aging Neurosci*. 2016;8(JUN):1-9. doi:10.3389/fnagi.2016.00139

2. Reijmer YD, Leemans A, Caeyenberghs K, Heringa SM, Koek HL, Biessels GJ. Disruption of cerebral networks and cognitive impairment in Alzheimer disease. *Neurology*. 2013;80(15):1370-1377. doi:10.1212/WNL.0b013e31828c2ee5

3. Pantoni L. Cerebral small vessel disease: from pathogenesis and clinical characteristics to therapeutic challenges. *Lancet Neurol*. 2010;9(7):689-701. doi:10.1016/S1474-4422(10)70104-6

4. Baykara E, Gesierich B, Adam R, et al. A Novel Imaging Marker for Small Vessel Disease Based on Skeletonization of White Matter Tracts and Diffusion Histograms. *Ann Neurol*. 2016;80(4):581-592. doi:10.1002/ana.24758

5. Van Der Flier WM, Skoog I, Schneider JA, et al. Vascular cognitive impairment. *Nat Rev Dis Prim*. 2018;4(Vci):1-16. doi:10.1038/nrdp.2018.3

6. Hagmann P, Kurant M, Gigandet X, et al. Mapping human whole-brain structural networks with diffusion MRI. *PLoS One*. 2007;2(7). doi:10.1371/journal.pone.0000597

7. Bozzali M, Falini A, Franceschi M, et al. White matter damage in Alzheimer's disease assessed in vivo using diffusion tensor magnetic resonance imaging. *J Neurol Neurosurg Psychiatry*. 2002;72(6):742-746. doi:10.1136/jnnp.72.6.742

8. Bosch B, Arenaza-Urquijo EM, Rami L, et al. Multiple DTI index analysis in normal aging, amnestic MCI and AD. Relationship with neuropsychological performance. *Neurobiol Aging*. 2012. doi:10.1016/j.neurobiolaging.2010.02.004

9. Serra L, Cercignani M, Lenzi D, et al. Grey and white matter changes at different stages of Alzheimer's disease. *J Alzheimer's Dis*. 2010. doi:10.3233/JAD-2010-1223

10. van Dellen E, Sommer IE, Bohlken MM, et al. Minimum spanning tree analysis of the human connectome. *Hum Brain Mapp*. 2018;39(6):2455-2471. doi:10.1002/hbm.24014

11. Fornito A, Zalesky A, Breakspear M. Graph analysis of the human connectome: Promise, progress, and pitfalls. *Neuroimage*. 2013;80:426-444. doi:10.1016/j.neuroimage.2013.04.087

12. Fan Y, Shi F, Smith JK, Lin W, Gilmore JH, Shen D. Brain anatomical networks in early human brain development. *Neuroimage*. 2011;54(3):1862-1871. doi:10.1016/j.neuroimage.2010.07.025

13. Otte WM, van Diessen E, Paul S, et al. Aging alterations in whole-brain networks during adulthood mapped with the minimum spanning tree indices: The interplay of density, connectivity cost and life-time trajectory. *Neuroimage*. 2015;109:171-189. doi:10.1016/j.neuroimage.2015.01.011

14. Daianu M, Jahanshad N, Nir TM, et al. Breakdown of brain connectivity between normal aging and Alzheimer's disease: A structural k-Core network analysis. *Brain Connect*. 2013;3(4):407-422. doi:10.1089/brain.2012.0137

15. Telesford QK, Simpson SL, Burdette JH, Hayasaka S, Laurienti PJ. The Brain as a Complex System: Using Network Science as a Tool for Understanding the Brain. *Brain Connect*. 2011;1(4):295-308. doi:10.1089/brain.2011.0055

16. van den Heuvel MP, Sporns O. Rich-club organization of the human connectome. *J Neurosci*. 2011;31(44):15775-15786. doi:10.1523/JNEUROSCI.3539-11.2011

17. Tzourio-Mazoyer N, Landeau B, Papathanassiou D, et al. Automated anatomical labeling of activations in SPM using a macroscopic anatomical parcellation of the MNI MRI single-subject brain. *Neuroimage*. 2002;15(1):273-289. doi:10.1006/nimg.2001.0978

18. van Wijk BCM, Stam CJ, Daffertshofer A. Comparing brain networks of different size and connectivity density using graph theory. *PLoS One*. 2010;5(10). doi:10.1371/journal.pone.0013701

19. Jones DK, Knösche TR, Turner R. White matter integrity, fiber count, and other fallacies: The do's and don'ts of diffusion MRI. *Neuroimage*. 2013;73:239-254. doi:10.1016/j.neuroimage.2012.06.081

20. Tewarie P, van Dellen E, Hillebrand A, Stam CJ. The minimum spanning tree: An unbiased method for brain network analysis. *Neuroimage*. 2015;104:177-188. doi:10.1016/j.neuroimage.2014.10.015

21. Buchanan CR, Bastin ME, Ritchie SJ, et al. The effect of network thresholding and weighting on structural brain networks in the UK Biobank. *bioRxiv*. 2019:649418. doi:10.1101/649418

22. Messaritaki E, Dimitriadis SI, Jones DK. Optimization of graph construction can significantly increase the power of structural brain network studies. *Neuroimage*. 2019;199:495-511. doi:10.1016/j.neuroimage.2019.05.052

23. Roine T, Jeurissen B, Perrone D, et al. Reproducibility and intercorrelation of graph theoretical measures in structural brain connectivity networks. *Med Image Anal*. 2019;52:56-67. doi:10.1016/j.media.2018.10.009

24. Serrano MÁ, Boguñá M, Vespignani A. Extracting the multiscale backbone of complex weighted networks. *Proc Natl Acad Sci U S A*. 2009;106(16):6483-6488. doi:10.1073/pnas.0808904106

25. van den Heuvel MP, Stam CJ, Boersma M, Hulshoff Pol HE. Small-world and scale-free organization of voxel-based resting-state functional connectivity in the human brain. *Neuroimage*. 2008;43(3):528-539. doi:10.1016/j.neuroimage.2008.08.010

26. Stam CJ, Tewarie P, Van Dellen E, van Straaten ECW, Hillebrand A, Van Mieghem P. The trees and the forest: Characterization of complex brain networks with minimum spanning trees. *Int J Psychophysiol*. 2014;92(3):129-138. doi:10.1016/j.ijpsycho.2014.04.001

27. Alvarez-Hamelin JI, Dall'Asta L, Barrat A, Vespignani A. Large scale networks fingerprinting and visualization using the k-core decomposition. *Adv Neural Inf Process Syst*. 2005:41-50.

28. Hagmann P, Cammoun L, Gigandet X, et al. Mapping the structural core of human cerebral cortex. *PLoS Biol*. 2008;6(7):1479-1493. doi:10.1371/journal.pbio.0060159

29. Aalten P, Ramakers IHGB, Biessels GJ, et al. The Dutch Parelsnoer Institute - Neurodegenerative diseases; methods, design and baseline results. *BMC Neurol*. 2014. doi:10.1186/s12883-014-0254-4

30. Van Essen D.C. et al. The Human Connectome Project: A data acquisition perspective. *2014 Jt Rail Conf JRC 2014*. 2012;62(4):2222-2231. doi:10.1115/JRC2014-3865

31. Van Den Berg E, Reijmer YD, De Bresser J, Kessels RPC, Kappelle LJ, Biessels GJ. A 4 year follow-up study of cognitive functioning in patients with type 2 diabetes mellitus. *Diabetologia*. 2010;53(1):58-65. doi:10.1007/s00125-009-1571-9

32. Schaefer A, Kong R, Gordon EM, et al. Local-Global Parcellation of the Human Cerebral Cortex from Intrinsic Functional Connectivity MRI. *Cereb Cortex*. 2018;28(9):3095-3114. doi:10.1093/cercor/bhx179

33. Dichgans M, Leys D. Vascular Cognitive Impairment. *Circ Res*. 2017;120(3):573-591. doi:10.1161/CIRCRESAHA.116.308426

34. Wardlaw JM, Valdés Hernández MC, Muñoz-Maniega S. What are white matter hyperintensities made of? Relevance to vascular cognitive impairment. *J Am Heart Assoc*. 2015;4(6):001140. doi:10.1161/JAHA.114.001140

35. Du J, Xu Q. Neuroimaging studies on cognitive impairment due to cerebral small vessel disease. *Stroke Vasc Neurol*. 2019;4(2):99-101. doi:10.1136/svn-2018-000209

36. Cordonnier C, Al-Shahi Salman R, Wardlaw J. Spontaneous brain microbleeds: Systematic review, subgroup analyses and standards for study design and reporting. *Brain*. 2007;130(8):1988-2003. doi:10.1093/brain/awl387

37. Debette S, Schilling S, Duperron MG, Larsson SC, Markus HS. Clinical Significance of Magnetic Resonance Imaging Markers of Vascular Brain Injury: A Systematic Review and Meta-analysis. *JAMA Neurol*. 2019;76(1):81-94. doi:10.1001/jamaneurol.2018.3122

38. Georgakis MK, Duering M, Wardlaw JM, Dichgans M. WMH and long-term outcomes in ischemic stroke: A systematic review and meta-analysis. *Neurology*. 2019;92(12):E1298-E1308. doi:10.1212/WNL.0000000000007142

39. van der Holst E. *Mind the Step in Cerebral Small Vessel Disease Disease*.; 2017.

40. Gouw AA, Seewann A, Van Der Flier WM, et al. Heterogeneity of small vessel disease: A systematic review of MRI and histopathology correlations. *J Neurol Neurosurg Psychiatry*.

2011;82(2):126-135. doi:10.1136/jnnp.2009.204685

41. Tuladhar AM, van Dijk E, Zwiers MP, et al. Structural network connectivity and cognition in cerebral small vessel disease. *Hum Brain Mapp*. 2016;37(1):300-310. doi:10.1002/hbm.23032

42. Kim HJ, Im K, Kwon H, et al. Clinical effect of white matter network disruption related to amyloid and small vessel disease. *Neurology*. 2015;85(1):63-70. doi:10.1212/WNL.0000000000001705

43. Lawrence AJ, Chung AW, Morris RG, Markus HS, Barrick TR. Structural network efficiency is associated with cognitive impairment in small-vessel disease. *Neurology*. 2014;83(4):304-311. doi:10.1212/WNL.0000000000000612

44. Haller S, Kövari E, Herrmann FR, et al. Do brain T2/FLAIR white matter hyperintensities correspond to myelin loss in normal aging? A radiologic-neuropathologic correlation study. *Acta Neuropathol Commun*. 2014;2(1):1-7. doi:10.1186/2051-5960-1-14

45. Lange N, Dubray MB, Lee JE, et al. Atypical diffusion tensor hemispheric asymmetry in autism. *Autism Res*. 2010;3(6):350-358. doi:10.1002/aur.162

46. Kubicki M, McCarley R, Westin CF, et al. A review of diffusion tensor imaging studies in schizophrenia. *J Psychiatr Res*. 2007;41(1-2):15-30. doi:10.1016/j.jpsychires.2005.05.005

47. Sexton CE, Kalu UG, Filippini N, Mackay CE, Ebmeier KP. A meta-analysis of diffusion tensor imaging in mild cognitive impairment and Alzheimer's disease. *Neurobiol Aging*. 2011;32(12):2322.e5-2322.e18. doi:10.1016/j.neurobiolaging.2010.05.019

48. Westlye LT, Walhovd KB, Dale AM, et al. Life-span changes of the human brain white matter: Diffusion tensor imaging (DTI) and volumetry. *Cereb Cortex*. 2010;20(9):2055-2068. doi:10.1093/cercor/bhp280

49. Brown BYR. A brief account of microscopical observations made on the particles contained in the pollen of plants. *Philos Mag*. 1828;4(21).

50. Einstein a. U¨ ber die von der molekularkinetischen Theorie der Wa¨ rme geforderte Bewegung von in ruhenden Flu¨ssigkeiten suspendierten Teilchen. *Ann d Phys*. 1905;322(8):549–560. doi:10.1002/andp.19053220806

51. Pierpaoli C, Jezzard P, Basser PJ, Barnett A DCG. Diffusion tensor MR imaging of the human brain. *Radiology*. 1996;14(4):514-520. doi:10.1097/00004728-199007000-00003

52. Sen PN, Basser PJ. A model for diffusion in white matter in the brain. *Biophys J*. 2005;89(5):2927-2938. doi:10.1529/biophysj.105.063016

53. Le Bihan D, Iima M. Diffusion magnetic resonance imaging: What water tells us about biological tissues. *PLoS Biol*. 2015;13(7):1-13. doi:10.1371/journal.pbio.1002203

54. Sandson TA, Felician O, Edelman RR, Warach S. Diffusion-Weighted Magnetic Resonance Imaging in Alzheimer ' s. 1999;02215:166-171.

55. Bastiani M, Roebroeck A. Unraveling the multiscale structural organization and connectivity of the human brain: The role of diffusion MRI. *Front Neuroanat*. 2015;9(June):1-15.

doi:10.3389/fnana.2015.00077

56. Johansen-Berg H, Behrens TEJ. *Diffusion MRI: From Quantitative Measurement to In Vivo Neuroanatomy: Second Edition*.; 2013. doi:10.1016/C2011-0-07047-3

57. Basser PJ, Mattiello J, LeBihan D. MR diffusion tensor spectroscopy and imaging. *Biophys J*. 1994;66(1):259-267. doi:10.1016/S0006-3495(94)80775-1

58. Alexander AL, Lee JE, Lazar M, Field AS. Diffusion Tensor Imaging of the Brain. 2007;4(July):316-329.

59. Curran K, Leemans A, Emsell L. Quantitative DTI measures. *ResearchGate*. 2016;(January):v-vii. doi:10.1007/978-1-4939-3118-7

60. Baliyan V, Das CJ, Sharma R, Gupta AK. Diffusion weighted imaging: Technique and applications. *World J Radiol*. 2016;8(9):785. doi:10.4329/wjr.v8.i9.785

61. Winston GP. The physical and biological basis of quantitative parameters derived from diffusion MRI. 2012;2(4):254-265. doi:10.3978/j.issn.2223-4292.2012.12.05

62. Mayo CD, Mazerolle EL, Ritchie L, Fisk JD, Gawryluk JR. Longitudinal changes in microstructural white matter metrics in Alzheimer's disease. *NeuroImage Clin*. 2017;13:330-338. doi:10.1016/j.nicl.2016.12.012

63. Kantarci K. Fractional anisotropy of the fornix and hippocampal atrophy in Alzheimer's disease. *Front Aging Neurosci*. 2014. doi:10.3389/fnagi.2014.00316

64. Selnes P, Aarsland D, Bjørnerud A, et al. Diffusion tensor imaging surpasses cerebrospinal fluid as predictor of cognitive decline and medial temporal lobe atrophy in subjective cognitive impairment and mild cognitive impairment. *J Alzheimer's Dis*. 2013;33(3):723-736. doi:10.3233/JAD-2012-121603

65. Basser PJ, Pajevic S, Pierpaoli C, Duda J, Aldroubi A. In vivo fiber tractography using DT-MRI data. *Magn Reson Med*. 2000;44(4):625-632. doi:10.1002/1522-2594(200010)44:4<625::AID-MRM17>3.0.CO;2-O

66. Jeurissen B, Descoteaux M, Mori S, Leemans A. Diffusion MRI fiber tractography of the brain. *NMR Biomed*. 2017;32(4):1-22. doi:10.1002/nbm.3785

67. Vos SB, Tax CMW, Leemans A. Diffusion magnetic resonance imaging and fiber tractography: The state of the art and its potential impact on patient management. *PET Clin*. 2013;8(3):279-293. doi:10.1016/j.cpet.2013.04.002

68. Rodrigues NB, Mithani K, Meng Y, Lipsman N, Hamani C. The emerging role of tractography in deep brain stimulation: Basic principles and current applications. *Brain Sci*. 2018;8(2). doi:10.3390/brainsci8020023

69. Sarwar T, Ramamohanarao K, Zalesky A. Mapping connectomes with diffusion MRI: deterministic or probabilistic tractography? *Magn Reson Med*. 2019;81(2):1368-1384. doi:10.1002/mrm.27471

70. Fornito A, Zalesky A, Bullmore E. *Fundamentals of Brain Network Analysis*.; 2016.

doi:10.1016/b978-0-12-407908-3.00001-7

71. Assaf Y, Johansen-Berg H, Thiebaut de Schotten M. The role of diffusion MRI in neuroscience. *NMR Biomed*. 2019;32(4):1-16. doi:10.1002/nbm.3762

72. Farquharson S, Tournier JD, Calamante F, et al. White matter fiber tractography: Why we need to move beyond DTI. *J Neurosurg*. 2013;118(6):1367-1377. doi:10.3171/2013.2.JNS121294

73. Behrens TEJ, Berg HJ, Jbabdi S, Rushworth MFS, Woolrich MW. Probabilistic diffusion tractography with multiple fibre orientations: What can we gain? *Neuroimage*. 2007. doi:10.1016/j.neuroimage.2006.09.018

74. Jeurissen B, Leemans A, Jones DK, Tournier JD, Sijbers J. Probabilistic fiber tracking using the residual bootstrap with constrained spherical deconvolution. *Hum Brain Mapp*. 2011;32(3):461-479. doi:10.1002/hbm.21032

75. Pierpaoli C, Barnett A, Pajevic S, et al. Water diffusion changes in wallerian degeneration and their dependence on white matter architecture. *Neuroimage*. 2001. doi:10.1006/nimg.2001.0765

76. Tournier JD, Calamante F, Connelly A. Robust determination of the fibre orientation distribution in diffusion MRI: Non-negativity constrained super-resolved spherical deconvolution. *Neuroimage*. 2007;35(4):1459-1472. doi:10.1016/j.neuroimage.2007.02.016

77. Tournier JD, Calamante F, Gadian DG, Connelly A. Direct estimation of the fiber orientation density function from diffusion-weighted MRI data using spherical deconvolution. *Neuroimage*. 2004;23(3):1176-1185. doi:10.1016/j.neuroimage.2004.07.037

78. Reijmer YD, Leemans A, Heringa SM, et al. Improved Sensitivity to Cerebral White Matter Abnormalities in Alzheimer's Disease with Spherical Deconvolution Based Tractography. *PLoS One*. 2012;7(8):1-8. doi:10.1371/journal.pone.0044074

79. Hagmann P. From diffusion MRI to brain connectomics. *Lausanne, EPFL*. 2005;9783642312:193-234. doi:10.1007/978-3-642-31208-3_6

80. Sporns O, Tononi G, Kötter R. The human connectome: A structural description of the human brain. *PLoS Comput Biol*. 2005;1(4):0245-0251. doi:10.1371/journal.pcbi.0010042

81. Bullmore E, Sporns O. Complex brain networks: Graph theoretical analysis of structural and functional systems. *Nat Rev Neurosci*. 2009;10(3):186-198. doi:10.1038/nrn2575

82. Reijmer YD, Leemans A, Brundel M, Kappelle LJ, Biessels GJ. Disruption of the cerebral white matter network is related to slowing of information processing speed in patients with type 2 diabetes. *Diabetes*. 2013;62(6):2112-2115. doi:10.2337/db12-1644

83. Telesford QK, Burdette JH, Laurienti PJ. An exploration of graph metric reproducibility in complex brain networks. *Front Neurosci*. 2013. doi:10.3389/fnins.2013.00067

84. Sotiropoulos SN, Zalesky A. Building connectomes using diffusion MRI: why, how and but. *NMR Biomed*. 2019;32(4):1-23. doi:10.1002/nbm.3752

85. Watts DJ, Strogatz SH. Strogatz - small world network Nature. *Nature*. 1998;393(June):440-

442. https://www.ncbi.nlm.nih.gov/pubmed/9623998.

86. Langer N, Pedroni A, Jancke L. The Problem of Thresholding in Small-World Network Analysis. 2013;8(2012). doi:10.1371/Citation

87. Lee UC, Mashour GA. Role of network science in the study of anesthetic state transitions. *Anesthesiology*. 2018;129(5):1029-1044. doi:10.1097/ALN.0000000000002228

88. Catani M, Ffytche DH. The rises and falls of disconnection syndromes. *Brain*. 2005;128(10):2224-2239. doi:10.1093/brain/awh622

89. Bullmore ET, Bassett DS. Brain Graphs: Graphical Models of the Human Brain Connectome. *Annu Rev Clin Psychol*. 2011;7(1):113-140. doi:10.1146/annurev-clinpsy-040510-143934

90. Rubinov M, Sporns O. Complex network measures of brain connectivity: Uses and interpretations. *Neuroimage*. 2010;52(3):1059-1069. doi:10.1016/j.neuroimage.2009.10.003

91. Stephan KE, Hilgetag CC, Burns GAPC, O'Neill MA, Young MP, Kötter R. Computational analysis of functional connectivity between areas of primate cerebral cortex. *Philos Trans R Soc B Biol Sci*. 2000;355(1393):111-126. doi:10.1098/rstb.2000.0552

92. Friston KJ, Tononi G, Sporns O, Edelman GM. Characterising the complexity of neuronal interactions. 1995.

93. Tononi G, Sporns O, Edelman GM. A measure for brain complexity: Relating functional segregation and integration in the nervous system. *Proc Natl Acad Sci U S A*. 1994;91(11):5033-5037. doi:10.1073/pnas.91.11.5033

94. Crossley NA, Mechelli A, Scott J, et al. The hubs of the human connectome are generally implicated in the anatomy of brain disorders. *Brain*. 2014;137(8):2382-2395. doi:10.1093/brain/awu132

95. Sporns O. The non-random brain: Efficiency, economy, and complex dynamics. *Front Comput Neurosci*. 2011;5(February):1-13. doi:10.3389/fncom.2011.00005

96. He Y, Dagher A, Chen Z, et al. Impaired small-world efficiency in structural cortical networks in multiple sclerosis associated with white matter lesion load. *Brain*. 2009;132(12):3366-3379. doi:10.1093/brain/awp089

97. Buckner RL, Sepulcre J, Talukdar T, et al. Cortical hubs revealed by intrinsic functional connectivity: Mapping, assessment of stability, and relation to Alzheimer's disease. *J Neurosci*. 2009;29(6):1860-1873. doi:10.1523/JNEUROSCI.5062-08.2009

98. Stam CJ. Modern network science of neurological disorders. *Nat Rev Neurosci*. 2014;15(10):683-695. doi:10.1038/nrn3801

99. De Brito Robalo BM, Vlegels N, Meier J, Leemans A, Biessels GJ, Reijmer YD. Effect of Fixed-Density Thresholding on Structural Brain Networks: A Demonstration in Cerebral Small Vessel Disease. *Brain Connect*. 2020;10(3):121-133. doi:10.1089/brain.2019.0686

100. Bullmore E, Sporns O. The economy of brain network organization. *Nat Rev Neurosci*. 2012;13(5):336-349. doi:10.1038/nrn3214

101. Goni J, Van Den Heuvel MP, Avena-Koenigsberger A, et al. Resting-brain functional connectivity predicted by analytic measures of network communication. *Proc Natl Acad Sci U S A*. 2014;111(2):833-838. doi:10.1073/pnas.1315529111

102. Stam CJ. Functional connectivity patterns of human magnetoencephalographic recordings: A "small-world" network? *Neurosci Lett*. 2004;355(1-2):25-28. doi:10.1016/j.neulet.2003.10.063

103. Van Den Heuvel MP, Kahn RS, Goñi J, Sporns O. High-cost, high-capacity backbone for global brain communication. *Proc Natl Acad Sci U S A*. 2012;109(28):11372-11377. doi:10.1073/pnas.1203593109

104. de Haan W, Van Der Flier WM, Wang H, Van Mieghem PFA, Scheltens P, Stam CJ. Disruption of Functional Brain Networks in Alzheimer's Disease: What Can We Learn from Graph Spectral Analysis of Resting-State Magnetoencephalography? *Brain Connect*. 2012;2(2):45-55. doi:10.1089/brain.2011.0043

105. Tijms BM, Möller C, Vrenken H, et al. Single-Subject Grey Matter Graphs in Alzheimer's Disease. *PLoS One*. 2013;8(3):1-9. doi:10.1371/journal.pone.0058921

106. Lo CY, Wang PN, Chou KH, Wang J, He Y, Lin CP. Diffusion tensor tractography reveals abnormal topological organization in structural cortical networks in Alzheimer's disease. *J Neurosci*. 2010;30(50):16876-16885. doi:10.1523/JNEUROSCI.4136-10.2010

107. Brier MR, Thomas JB, Fagan AM, Hassenstab J, David M. Functional connectivity and graph thery in preclinical Alzheimer ' s disease. *Elsevier*. 2014;(4):1-25. doi:10.1016/j.neurobiolaging.2013.10.081.Functional

108. Shu N, Liang Y, Li H, et al. Disrupted Topological Organization in White Matter Structural Networks in Amnestic Mild Cognitive Impairment. *Neuroradiology*. 2012;265(2):518-527. doi:10.1148/radiol.12112361/-/DC1

109. Kruskal JB. On the Shortest Spanning Subtree of a Graph and the Traveling Salesman Problem. *Proc Am Math Soc*. 1956;7(1):48. doi:10.2307/2033241

110. Bender EA, Williamson SG. Lists , Decisions and Graphs With an Introduction to Probability Unit DT : Decision Trees and Recursion Edward A . Bender. 2010.

111. Wang H, Hernandez JM, Van Mieghem P. Betweenness centrality in a weighted network. *Phys Rev E - Stat Nonlinear, Soft Matter Phys*. 2008;77(4):1-10. doi:10.1103/PhysRevE.77.046105

112. Boersma M, Smit DJ a., Boomsma DI, de Geus EJ c., delemarre-Van de Waal HA, Stam CJ. Growing Trees in Child Brains: Graph Theoretical Analysis of Electroencephalography-Derived Minimum Spanning Tree in 5- and 7-Year-Old Children Reflects Brain Maturation. *Brain Connect*. 2013;3(1):50-60. doi:10.1089/brain.2012.0106

113. Dellen E Van, Douw L, Hillebrand A, et al. Epilepsy surgery outcome and functional network alterations in longitudinal MEG: A minimum spanning tree analysis. *Neuroimage*. 2014.

114. Sporns O, Honey CJ, Kötter R. Identification and classification of hubs in brain networks. *PLoS One*. 2007. doi:10.1371/journal.pone.0001049

115. Colizza V, Flammini A, Serrano MA, Vespignani A. Detecting rich-club ordering in complex networks. *Nat Phys*. 2006;2(2):110-115. doi:10.1038/nphys209

116. Opsahl T, Colizza V, Panzarasa P, Ramasco JJ. Prominence and control: The weighted rich-club effect. *Phys Rev Lett*. 2008;101(16):1-4. doi:10.1103/PhysRevLett.101.168702

117. Morris JC. The clinical dementia rating (cdr): Current version and scoring rules. *Neurology*. 1993. doi:10.1212/wnl.43.11.2412-a

118. Folstein MF, Folstein SE, McHugh PR. "Mini-mental state". A practical method for grading the cognitive state of patients for the clinician. *J Psychiatr Res*. 1975. doi:10.1016/0022-3956(75)90026-6

119. Leemans A, Jeurissen B, Sijbers J, Jones DK. ExploreDTI: a graphical toolbox for processing, analyzing, and visualizing diffusion MR data. *Proc Int Soc Magn Reson Med*. 2009;17(2):3537.

120. Tax CMW, Otte WM, Viergever MA, Dijkhuizen RM, Leemans A. REKINDLE: Robust Extraction of Kurtosis INDices with Linear Estimation. *Magn Reson Med*. 2015. doi:10.1002/mrm.25165

121. Odish OFF, Caeyenberghs K, Hosseini H, Van Den Bogaard SJA, Roos RAC, Leemans A. Dynamics of the connectome in Huntington's disease: A longitudinal diffusion MRI study. *NeuroImage Clin*. 2015. doi:10.1016/j.nicl.2015.07.003

122. Brandes U. A faster algorithm for betweenness centrality. *J Math Sociol*. 2001. doi:10.1080/0022250X.2001.9990249

123. Sørensen T. A method of establishing groups of equal amplitude in plant sociology based on similarity of species content, and its application to analyses of the vegetation on Danish commons. *K Danske Vidensk Selsk Biol Skr*. 1948.

124. Dice LR. Measures of the Amount of Ecologic Association Between Species. *Ecology*. 1945. doi:10.2307/1932409

125. Kellaway FW, Kreyszig E. Advanced Engineering Mathematics. *Math Gaz*. 1969. doi:10.2307/3612523

126. Reijmer YD, Fotiadis P, Martinez-Ramirez S, et al. Structural network alterations and neurological dysfunction in cerebral amyloid angiopathy. *Brain*. 2015. doi:10.1093/brain/awu316

127. Sporns O. Contributions and challenges for network models in cognitive neuroscience. *Nat Neurosci*. 2014. doi:10.1038/nn.3690

8. Appendix

Table A.1 - Mathematical definitions of complex network measures. From the paper of Tewarie *et al.*[20]. The Brain Connectivity Toolbox contains Matlab functions to compute most measures in this table.

Symbol	Concept	Explanation	Formula
N	Nodes	Number of nodes	
M	Links	Number of links/maximum leaf number	
k	Degree	Number of links for a given node	$k_i = \sum_{j \in N} a_{ij}$
C	Clustering coefficient	C is a measure of the local connectedness of a network, which is defined as the fraction of triangles in the network	$C = \frac{1}{N}\sum_{i \in N} \frac{\sum_{j,h \in N} a_{ij} a_{ih} a_{jh}}{k_i(k_i-1)}$ a corresponds to links connecting node i, j or h
C_W	Weighted clustering coefficient	C_w is the clustering coefficient for weighted networks	$C_w = \frac{1}{N}\sum_{i \in N} \frac{\sum_{j,h \in N} \left(w_{ij} w_{ih} w_{jh}\right)^{1/3}}{k_i(k_i-1)}$ w corresponds to links connecting node i, j or h
L	Path length	L is defined as the average shortest path between any two nodes in the network. The paths are based on the topological distance between nodes d_{ij}, where distance is defined as the inverse of the link weights	$L = \frac{1}{N}\sum_{i \in N} \frac{\sum_{j \in N, j \neq i} d_{ij}}{n-1}$
L_W	Weighted path length	L_w is the weighted form of the path length in case that the network of interested is weighted	$L_w = \frac{1}{N}\sum_{i \in N} \frac{\sum_{j \in N, j \neq i} d_{ij}^{W}}{n-1}$
L_f	Leaf fraction	Fraction of leaf nodes (L) in the MST where a leaf node is defined as a node with degree one	$L_f = L/M$
D	Diameter	Longest shortest path d of an MST. The diameter is also related to the leaf number. The upper limit of the diameter is defined as $d_{max} = m - L + 2$, which implies that the value of the largest possible diameter decreases when the leaf number increases	$D = d/M$
	Eccentricity	Longest shortest path from a reference node to any other node in the MST. The eccentricity of the whole MST is the difference between the eccentricity values of the nodes with the largest and smallest eccentricity in the tree	
BC	Betweenness centrality	Fraction of all shortest paths that pass through a particular node	$BC_i = \frac{1}{(n-1)(n-2)} \sum_{\substack{h,j \in N \\ h \neq j, h \neq i, \neq i}} \frac{\rho_{hj}^{(i)}}{\rho_{hj}}$ ρih is the number of shortest paths between h and j, and ρih(i) is the number of shortest paths between h and j that pass through i.
κ	Degree divergence	Measure of the broadness of the degree distribution. Related to resilience against attacks, epidemic spreading and the synchronizability of complex networks	$\kappa = \frac{\langle k^2 \rangle}{\langle k \rangle}$
Th	Tree hierarchy	Quantifies the trade-off between large scale integration in the MST and the overload of central nodes	$T_H = \frac{L}{\sum BC_{max}}$
	Overlap	The fraction of links that two MSTs (MST_x and MST_y) have in common. This value can range between 0 and 1.	$Overlap = \frac{MST_x \cap MST_y}{M}$

Table A.2 – Mathematical definitions of shortest path length and global efficiency measures, from Rubinov and Sporns[90]. The Brain Connectivity Toolbox contains Matlab functions to compute the measures in this table.

Measure	Binary and undirected definitions	Weighted and directed definitions
Shortest path length: a basis for measuring integration	Shortest path length (distance), between nodes i and j, $d_{ij} = \sum_{a_{uv} \in g_{i \leftrightarrow j}} a_{uv}$, where $g_{i \leftrightarrow j}$ is the shortest path (geodesic) between i and j. Note that $d_{ij} = \infty$ for all disconnected pairs i, j.	Shortest weighted path length between i and j, $d_{ij}^{W} = \sum_{a_{uv} \in g_{i \leftrightarrow j}^{W}} f(w_{uv})$, where f is a map (e.g., an inverse) from weight to length and $g_{i \leftrightarrow j}^{W}$ is the shortest weighted path between i and j. Shortest directed path length from i to j, $d_{ij}^{\rightarrow} = \sum_{a_{ij} \in g_{i \rightarrow j}} a_{ij}$, where $g_{i \rightarrow j}$ is the directed shortest path from i to j.
Global efficiency	Global efficiency of the network (Latora and Marchiori, 2001), $E = \frac{1}{n}\sum_{i \in N} E_i = \frac{1}{n}\sum_{i \in N} \frac{\sum_{j \in N, j \neq i} d_{ij}^{-1}}{n-1}$, where E_i is the efficiency of node i.	Weighted global efficiency, $E^{W} = \frac{1}{n}\sum_{i \in N} \frac{\sum_{j \in N, j \neq i} \left(d_{ij}^{W}\right)^{-1}}{n-1}$. Directed global efficiency, $E^{\rightarrow} = \frac{1}{n}\sum_{i \in N} \frac{\sum_{j \in N, j \neq i} \left(d_{ij}^{\rightarrow}\right)^{-1}}{n-1}$.